NOAA Technical Memorandum NMFS-AFSC-525

A revised time series of euphausiid density and distribution from acoustic-trawl surveys of the Eastern Bering Sea shelf

M. Levine, A. De Robertis, P. Ressler, and B. Lucca

August 2026

U.S. DEPARTMENT OF COMMERCE

National Oceanic and Atmospheric Administration
National Marine Fisheries Service
Alaska Fisheries Science Center

The National Marine Fisheries Service's Alaska Fisheries Science Center uses the NOAA Technical Memorandum series to issue informal scientific and technical publications when complete formal review and editorial processing are not appropriate or feasible. Documents within this series reflect sound professional work and may be referenced in the formal scientific and technical literature.

The NMFS-AFSC Technical Memorandum series of the Alaska Fisheries Science Center continues the NMFS-F/NWC series established in 1970 by the Northwest Fisheries Center. The NMFS-NWFSC series is currently used by the Northwest Fisheries Science Center.

This document should be cited as follows:

Levine, M., De Robertis, A., Ressler, P., Lucca, B. 2026. A revised time series of euphausiid density and distribution from acoustic-trawl surveys of the Eastern Bering Sea shelf. U.S. Department of Commerce, NOAA Technical Memorandum NMFS-AFSC-525, 86 p.

This document is available online at:

Document available: https://repository.library.noaa.gov

Reference in this document to trade names does not imply endorsement by the National Marine Fisheries Service, NOAA.

NOAA FISHERIES

A revised time series of euphausiid density and distribution from acoustic-trawl surveys of the Eastern Bering Sea shelf

M. Levine[1], A. De Robertis[1], P. Ressler[1], and B. Lucca[2]

[1]Alaska Fisheries Science Center
National Marine Fisheries Service
National Oceanic and Atmospheric Administration
7600 Sand Point Way N.E.
Seattle, WA 98115-6349

[2]Fisheries Collaborative Program
University of California, Santa Cruz
In collaboration with NOAA's Southwest Fisheries Science Center
2725 Montlake Blvd. E.
Seattle, WA 98112-2013

U.S. DEPARTMENT OF COMMERCE

National Oceanic and Atmospheric Administration National Marine Fisheries Service
Alaska Fisheries Science Center

NOAA Technical Memorandum NMFS-TM-AFSC-525

August 2026

U.S. Secretary of Commerce
Howard Lutnick

Under Secretary of Commerce
for Oceans and Atmosphere
Neil Jacobs

Assistant Administrator, National
Marine Fisheries Service.
Eugenio Piñeiro Soler

August 2026

www.nmfs.noaa.gov

OFFICIAL BUSINESS

National Marine
Fisheries Service
Alaska Fisheries Science Center
7600 Sand Point Way N.E.
Seattle, WA 98115-6349

Table of Contents

Updated EBS euphausiid time series: key improvements and changes 1

Introduction *1*

Updated method: changes to the existing method *3*

Updated method: summary *7*

Updated method: data access *8*

Tables and figures *11*

Appendix I: Methodological changes 15

Summary of the historical method *15*

Updates to the historical method *17*

Results and Discussion *28*

Summary: processing steps in the updated method *37*

Appendix I Tables and Figures *39*

Appendix II: modeling krill TS 53

Introduction *53*

SDWBA model parameterization *55*

Implementation using acousticTS in R *59*

Appendix II Tables and Figures *69*

Acknowledgments 75

References 77

Updated EBS euphausiid time series: key improvements and changes

Introduction

Euphausiids (primarily *Thysanoessa raschii* and *T. inermis,* hereafter referred to as krill) are a major trophic link in the Eastern Bering Sea (EBS) ecosystem. Krill are a primary prey item for fishes including walleye pollock (Gadus chalcogrammus, hereafter referred to as pollock; Brodeur et al. 2002, Lang et al. 2005), birds including short-tailed shearwaters (Ardenna tenuirostris; Hunt et al. 2002, Nishizawa et al. 2017) and murres (Uria spp.; Decker and Hunt 1996), and fin (Balaenoptera physalus) and humpback (Megaptera novaengliae) whales (Witteveen et al. 2015). Estimates of EBS krill abundance and distribution are utilized in pollock fishery stock assessments (Ianelli et al. 2024), ecosystem-based fishery management efforts (Siddon 2024), and investigations of krill-pollock population dynamics (Ressler et al. 2014, Hunt et al. 2016).

The Alaska Fisheries Science Center Midwater Assessment and Conservation Engineering (MACE) Program has produced a time series of krill density since 2004 (Ressler et al. 2012, Levine and Ressler 2024). This time series is based on data collected during biennial acoustic-trawl surveys of the EBS shelf. While these surveys are primarily designed to assess pollock distribution and abundance, they additionally collect multifrequency acoustic data at frequencies ranging from 18 to 200 kHz. These multifrequency data are useful for acoustically differentiating krill from other common midwater species groups as backscatter from krill is stronger at higher frequencies than at lower frequencies, while backscatter from swim-bladdered fish species is not (Cochrane et al. 1991, Holliday and Pieper 1995, De Robertis et al. 2010). This characteristic allows pairwise differences in backscattering strength at each combination of acoustic

frequencies ("dB-differencing") to be compared to expected differences from trawl-verified samples dominated by krill, yielding estimates of acoustic backscatter attributed to krill (De Robertis et al. 2010, Ressler et al. 2012, Simonsen et al. 2016).

For many applications, estimates of krill density or biomass are more directly relatable to ecosystem processes than estimates of krill acoustic backscatter. Converting from acoustic backscatter to units of density or biomass requires both information on the species and size composition of the animals responsible for the acoustic scattering as well as knowledge of the amount of backscatter reflected from individuals from each species and size class (i.e. 'target strength,' hereafter TS, Simmonds and MacLennan 2005). In the EBS krill time series, information on species and size composition is obtained by directed trawling on acoustically observed krill layers (Ressler et al. 2012). Krill TS is dependent on animal shape and length, orientation in relation to the acoustic beam, density and sound speed contrasts with the surrounding seawater, and the acoustic frequency at which the animal is insonified (Stanton et al. 1993, Stanton and Chu 2000). The EBS time series has utilized a TS model parameterized with size and material properties from sampled Bering Sea krill (Smith 2010, Ressler et al. 2012, Smith et al. 2013). The resulting density calculations are subject to considerable uncertainty in the size, morphology, material properties and *in situ* orientation of krill, with ~10 dB variation in krill TS at 120 kHz depending on the selection of parameters (Ressler et al. 2012, Smith et al. 2013). These uncertainties motivated recent work collecting additional measurements of material properties, *in situ* orientation, and krill body shape in EBS krill species (Lucca et al. 2021, 2023).

Here, we summarize a series of updates to the methods used to generate this time series. The updates affect the backscatter-to-density and backscatter-to-biomass conversion process, the acoustic krill identification process, and the index standardization process. The updates were

motivated by incremental improvements to acoustic data processing and krill identification techniques that have occurred since the methodology was first developed in 2012, a review of our use of krill trawl catch data to convert acoustic backscatter, and recent work which improved estimates of krill TS in the EBS. In addition to these methodological updates, we were motivated to make the methodology underlying this time series of spatially explicit estimates of krill density more transparent and to make it publicly available.

We first describe the major changes to the time series resulting from these updates in general terms (see **Updated method: summary** and **Updated method: data access** below). For many users of the updated time series, this section will provide a sufficient introduction to the methodology. We then describe the rationale, implementation, and effects of each specific update in more detail for the interested reader (see **Appendix I** and **Appendix II**).

Updated method: changes to the existing method

The updated method incorporated six changes to the acoustic krill identification process, three changes to the backscatter-to-density and -biomass conversion process, and one change to the index standardization process (see **Appendix I** and **Appendix II** for details). To explore the magnitude of each change, we conducted a series of comparisons with the existing method (hereafter referred to as the 'historical method'). These comparisons indicated that updates to the backscatter-to-density and -biomass conversion process had a much greater effect on estimates than updates to the acoustic identification process or index standardization process (Figure 1; Table 1).

Conversion from backscatter to density and biomass

As compared to the large volume of acoustic data (collected over 2,500 to 5,000+ nautical miles (nmi) of transect line, depending on the survey year), the number of trawls used to sample the species and size composition of acoustically observed krill layers is comparatively low (a mean of 10 trawls per year, ranging from 1 to 24 trawls per year). Given the limited trawl information available, the historical method used pooled multi-year averages of krill length to apply a single TS model (Smith et al. 2013) for the EBS. The historical method additionally applied this model separately in two depth strata based on a long-term pattern in krill species distribution, with *T. inermis* primarily found in deeper strata and *T. raschii* found in shallower strata (this accounted for potential differences in length distributions between these species, though density and biomass estimates are made for all krill, and are not species-specific; Ressler et al. 2012, Levine and Ressler 2024). However, pooling length estimates among years may miss inter-annual and longer term changes in length composition, including those driven by climate change (Mueter and Litzow 2008, Michael et al. 2021, Rooper et al. 2021, Levine et al. 2023). Additionally, given that the EBS krill time series now spans 20 years and the total number of trawl samples is larger than it was when the historical method was initially developed, there are more available data to examine how the targeted krill trawl information should be used than when the historical method was established.

In terms of species composition, krill dominated Methot trawl catches, the majority of the species captured were *T. raschii* and *T. inermis*, and there was no evidence of a clear change in krill species composition over the time series. However, changes in annual mean krill length (average ~19 mm, varying by ~3.5 mm over the 2004 to 2024 dataset) were substantial despite low sample size and high variability. We therefore decided to use the annual mean krill length to

apply krill TS models as opposed to using a long-term mean length. Using annual estimates of mean length produced krill density estimates that differed appreciably from those made using the historic method of pooling lengths across years. Mean survey-level krill density changed by an average of 22.4% over the survey years (range: -30.3 to 95.8%; Figure 1, Table 1). In periods when krill were larger than the long-term mean length (including the years 2009 to 2014), the use of annual length estimates lowered densities estimates relative to the historical method: estimates declined by 11.0 to 30.3% using annually estimated lengths as compared to using the long-term mean length because the estimated acoustic backscatter per krill increased. Conversely, in periods when krill were smaller in size (including the years 2016 to 2024), krill densities increased (2016 to 2024 estimates increased by 48.1 to 95.8%; Figure 1, Table 1).

As compared to the Smith et al. (2013) TS model used in the historical approach, the updated TS model (Lucca et al. 2021; for details on parameterization see **Appendix II**) indicates that krill are stronger scatterers at all length classes. At the range of lengths observed in the 2004 to 2024 catch data (annual mean krill length 16.7 mm to 20.7 mm), this corresponds to a 4.5 dB to 6.9 dB increase in TS in the updated TS model as compared to the historical model. The increase in TS led to a corresponding decrease in krill density: krill density declined on average by 71.3% (-79.4 to -64.1%) relative to the historical method (Figure 1, Table 1). However, the relative interannual pattern (i.e. 'high' years and 'low' years) is consistent between the historical and the updated methods (Figure 2).

Acoustic identification of krill

The impact of changes to the acoustic identification process were relatively small (Figure 1, Table 1) but added meaningful improvements to the time series. For example, the addition of the

70 kHz frequency for multifrequency identification provided an additional, useful contrast in differentiating krill from pollock (De Robertis et al. 2010), resulting in more precise krill identification. Similarly, updates to the 'shadow correction,' which estimates the effect of comparatively strong pollock 'shadowing' krill when both taxa co-occur and applies a backscatter correction proportional to the extent of the shadowing, removed a persistent low bias in the historical method and increased krill backscatter.

Other changes integrated improvements in monitoring and mitigating for acoustic noise that have had negligible effects on the time series but could become important in future surveys. For example, we now provide methods that allow for the 200 kHz frequency to 'fill in' in cases where the 120 kHz is not available, and methods that assess acoustic noise at all frequencies (background noise at 18 and 38 kHz was assumed to be negligible). Although these improvements make little difference to the revised time series, as these assumptions are largely met, they make the analyses more robust to issues that may arise in future acoustic measurements.

Index standardization

We standardized the time series survey area by limiting the survey domain to the core area which is sampled in all years. This makes the data more comparable across years; though it has little impact on the current time series (Figures 1, 2), it could be more important if the survey spatial domain changes in the future.

Updated method: summary

The revised annual krill density and biomass estimates differ from those made using historical methods. This is due primarily to updates to the krill backscatter-to-density conversion process. While the historical and the updated krill backscatter time series produce similar estimates of krill backscatter (Figure 2a), the updated krill volumetric density, areal density, and wet weight time series are substantially lower than the historical versions (Figure 2b, c, d). That said, the relative interannual pattern (e.g., 'high' and 'low' years) remains mostly the same between the time series versions.

The reduction in the updated metrics of krill density and biomass was due to the new TS-length relationship (Lucca et al. 2021) used to convert backscatter to density (Figure 1). Additionally, the sizeable effect of krill length estimates on the krill indices (Figure 1) highlights the importance of size composition data obtained from trawl sampling and the need to better quantify and characterize this uncertainty. To reduce this uncertainty, future surveys should sample krill in areas of high abundance throughout the entire survey area, either through targeted trawls or through emerging optical (Levine et al. 2018, Svantemann et al. 2025) or acoustic (i.e. broadband acoustic measurements, Amakasu et al. 2017) methods. Increased biological sampling effort could allow for species-specific krill estimates to be produced in the EBS.

The updated estimates help resolve a long-standing issue in krill survey methodology: acoustic surveys often produce estimates that are an order of magnitude greater than net-based surveys (Coyle 2000, Hunt et al. 2016). This has been attributed to diverging biases in each approach, with net estimates negatively biased due to krill plankton net avoidance (Sameoto 1980) and acoustic estimates positively biased due to uncertainties in the proportion of backscatter that

stems from krill and the TS of krill (Stanton and Chu 2000). In the historical EBS time series, surveys from 2004 to 2010 produced an average acoustic density of ~30 krill m^{-3} and an average net-based estimate of ~4 krill m^{-3} (Ressler et al. 2012), while the updated method produces an average estimate of 13 krill m^{-3} over this time frame. This reduces the discrepancies, which are within the range expected due to the relatively large potential effects of net avoidance and TS uncertainty (Hunt et al. 2016, their Appendix A).

Updated method: data access

Because krill density and distribution in the EBS is of interest to researchers working on ecosystem processes as well as those conducting analyses for ecosystem-based fisheries management efforts, we have shared the EBS krill time series in a publicly accessible repository. The MACE KrillCommunication repository (https://github.com/noaa-afsc-mace/KrillCommunication) shares krill estimates from all EBS summer surveys from 2004 to 2024, including data from a 2020 survey that was conducted using Saildrone uncrewed surface vehicles (Levine and De Robertis 2025).

The data are reported in units of krill backscatter (Nautical Area Scattering Coefficient, s_A, m^2 nmi^{-2}), krill volumetric density (individuals m^{-3}), krill areal density (individuals m^{-2}), and krill wet weight (g m^{-2}). We provide data at three spatial scales: totals per survey year (useful for ecosystem-scale interannual patterns), vertically integrated at 0.5 nmi horizontal resolution along acoustic transects (useful for 2-dimensional spatial krill distributions), and 0.5 nmi horizontal × 20 m vertical resolution (useful for both the horizontal and vertical distribution of krill). Additionally, we provide metadata and example scripts to allow researchers to more easily use

this dataset. KrillCommunication is intended to be updated biennially as additional EBS summer surveys are conducted.

Tables and figures

Table 1. Summary of changes in the updated krill method. Each addition is briefly summarized; see Appendix I for details. Effect is presented as the mean and range (%) of the addition in comparison to the most relevant reference point (reference points are *italicized* within table). Addition type "Acoustic" indicates a change to the acoustic identification process, addition type "Core survey grid" indicates a standardization of the survey domain, and addition type "Conversion" indicates a change to the backscatter-to-density and -biomass conversion process. See Figure 2 for a summary of the relative effect of each addition.

Addition	Addition type	Summary: Historical method	Summary: Updated method	Effect (%)	Figure
Signal-to-noise ratio (SNR)	Acoustic	Did not check SNR at all frequencies	Check SNR at all frequencies; uses improved passive noise estimation	1.1 [-2.1 to 6.9]; *Historical method mean* s_A	A1.1
New base	Acoustic	Export 120 kHz S_v attributed to krill at 0.5 nmi horizontal × 20 m vertical resolution	Export S_v from all frequencies at 5 ping horizontal × 5 m vertical resolution for more flexible processing; small error fixes in past surveys	-1.9 [-12.7 to 4.3]; *Historical method mean* s_A	A1.2
+ 200 kHz	Acoustic	Require valid 120 kHz S_v value for krill cells	Allow for cases with valid 200 kHz S_v but not 120 kHz S_v; adjust 200 kHz to 120 kHz equivalent for integration	0.3 [0.0 to 1.8]; *New base*	A1.2
+ 70 kHz	Acoustic	4 frequencies (18, 38, 120, 200 kHz) used for krill identification	5 frequencies (18, 38, 70, 120, 200 kHz) used for krill identification	-11.0 [-22.6 to -5.1]; *200 kHz for integration*	A1.2
Shadow correction	Acoustic	Resolution of the shadow correction for pollock overlap did not match resolution for krill identification (error in historical method)	Resolution of the shadow correction for pollock overlap matches resolution for krill identification	9.8 [4.9 to 16.4]; *70 kHz for identification*	A1.2

Addition	Addition type	Summary: Historical method	Summary: Updated method	Effect (%)	Figure
≥ 2 neighbors	Acoustic	Remove marginal krill using statistical criteria (large-scale Z-score)	Remove marginal krill by requiring krill cells to be co-located (consistent with krill layering)	-1.7 [-5.5 to 1.7]; *Z-score based krill removal*	A1.3
Core survey grid	Index Standardization	Krill index based on all observations (inside and outside the core survey area)	Krill index based on observations within a consistently sampled core survey area	-1.0 [-8.4 to 6.0]; *Index based on all observations*	A1.2
TS-Length model	Conversion	Smith et al. (2013) model parameterized based on EBS krill collections, but considerable uncertainty in measurement of material properties and *in-situ* krill orientation.	Lucca et al. (2021, 2023) model parameterized based on expanded EBS specimen collection, *in-situ* krill orientation, and comparisons of model predictions and experimental measurements; model fit using observed parameter distributions.	-71.3 [-79.4 to -64.1] *Krill density in the core EBS calculated with Smith 2013 vs Lucca 2021, 2023*	A1.11
Annual krill length	Conversion	Mean krill length determined from multi-year average	Mean krill length determined on a per-year basis	22.4 [-30.3 to 95.8]; *Historical krill density in the core EBS (m^3) calculated using multi-year average*	A1.7; A1.8b
No depth strata	Conversion	Mean krill length determined for inshore (< 100 m depth) and offshore (> 100 m depth) strata	Mean krill length determined for entire EBS shelf (no depth strata)	-0.7 [-4.5 to 6.5]; *mean krill length determined by depth strata*	A1.8a

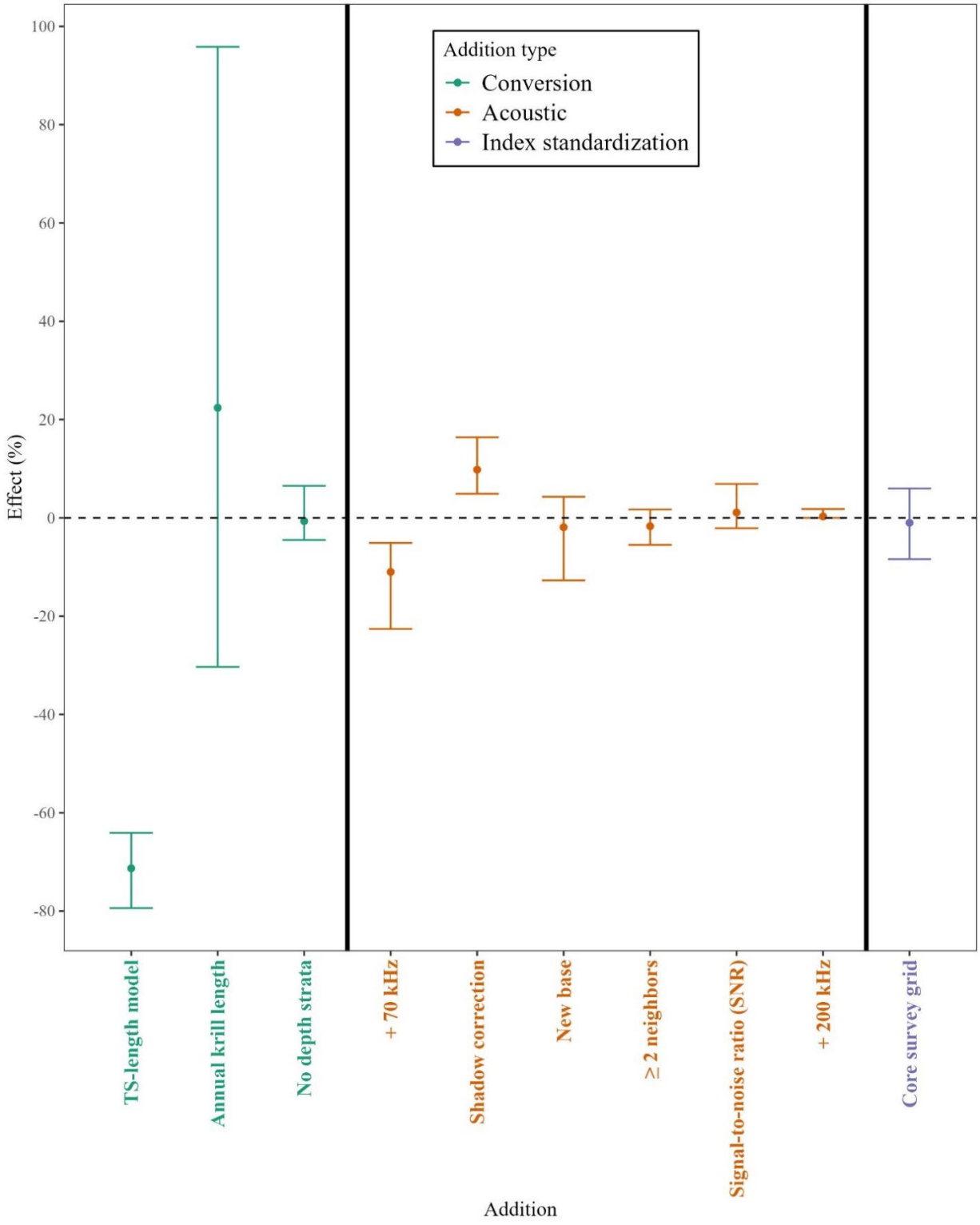


Figure 1. Relative effect of each methodological addition. Changes are reported as the mean percent change (points) and range (error bars) for each addition, in relation to an appropriate reference point. See Table 1 for more detail on each addition type and reference point.

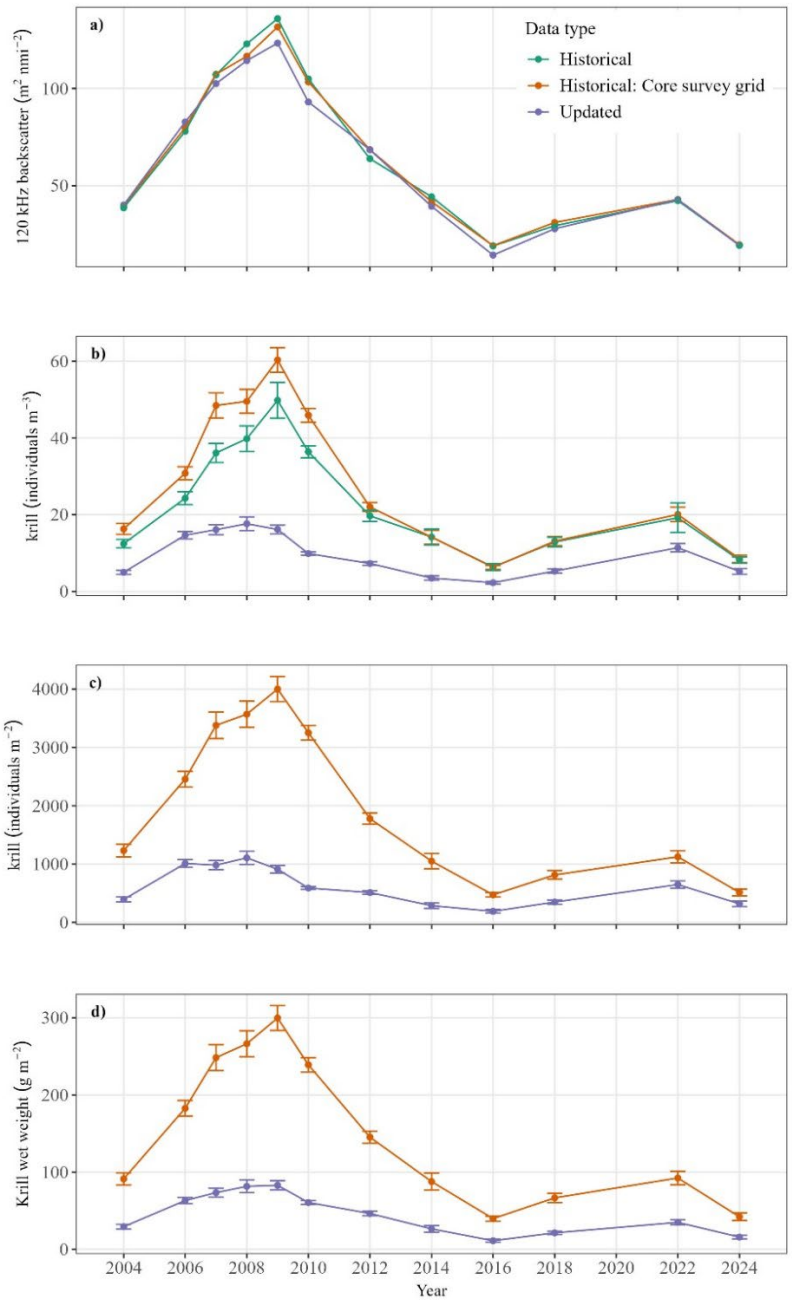


Figure 2. Time series comparison. “Historical” refers to estimates previously calculated using the historical processing method, ‘Historical: Core survey grid’ refers to estimates generated using the historical method but re-calculated within a standard survey footprint, and ‘Updated’ refers to estimates made using the updated processing method. Estimates are presented in units of a) krill backscatter (m^2 nmi^{-2}), b) krill volumetric density (m^{-3}), c) krill areal density (m^{-2}), and krill wet weight (g m^{-2}). Error bars represent 95% confidence intervals on units of density and wet weight calculated using a geostatistical estimate of sampling error. Note that “Historical” values were only available in units of backscatter and volumetric density (the values historically provided within Ecosystem Status Reports).

Appendix I: Methodological changes

Summary of the historical method

The historical method is fully described in De Robertis et al. (2010) and Ressler et al. (2012) and is summarized here. Acoustic scatterers are identified by comparing their relative frequency response across 4 acoustic frequencies (18, 38, 120, and 200 kHz) with those of known scattering groups. Acoustic backscatter (mean volume backscattering strength, S_v, dB re 1 m^{-1}; for descriptions of all acoustic units used in our processing refer to MacLennan et al. 2002) was averaged into 5 m vertical × 5 ping horizontal cells at each frequency. To avoid biasing cells with background noise, the signal-to-noise ratio (SNR) was then calculated at 120 and 200 kHz (De Robertis and Higginbottom 2007), and only cells with SNR ≥ 10 dB were retained. Similarly, measurements made at 18 kHz can be biased by ringing noise from the transmit pulse, especially at closer ranges to the transducer (ringing noise is range dependent, with S_v from ringing decaying linearly with range). Therefore, only 18 kHz cells with a SNR ≥ 10 dB above the ringing noise were retained (Ressler et al. 2012).

Pairwise frequency differences were then calculated for S_v measurements made at 18, 38, 120, and 200 kHz (i.e. ΔS_v, where for each frequency pair i,j, $\Delta S_{V,i-j}=S_{V,i}-S_{V,j}$; De Robertis et al. 2010). This yielded 6 ΔS_v values in cells with 4 valid S_v measurements (because the historical method allowed cases where either the 18 or the 200 kHz value was missing due to low SNR to be included, there are cells with < 6 ΔS_v values). ΔS_v values were then compared to ΔS_v values of known taxa (pollock, krill, jellyfish, and myctophids; De Robertis et al. 2010), producing measurements of the deviation from the expectation for each ΔS_v measurement and taxon ('Z-score'; De Robertis et al. 2010). For each cell, the Z-score for each known taxon was then

summarized as the mean absolute value of all Z-scores for that taxon (i.e. in a cell with 4 valid S_v measurements, the Z-score would be the mean absolute value of the 6 individual Z-scores). Cells where the mean krill Z-score was ≤ 2 and the mean krill Z-score was lower than that of all other taxa were identified as krill. These cells were then integrated into larger 0.5 nmi horizontal × 20 m vertical elementary distance sampling units (EDSUs; Simmonds and MacLennan 2005) from 20 m below the surface to 0.5 m above the seafloor at 120 kHz with an integration threshold of -80 dB re 1 m^{-1}. To remove EDSUs with marginal krill identifications, the mean Z-score of cells in the 0.5 nmi × 20 m EDSUs was then calculated, and only EDSUs with a mean Z-score ≤ 1.5 were retained as krill.

Two corrections were then applied to krill backscatter. Data from before sunrise and after sunset were removed due to krill diel vertical migration behavior (Mauchline 1980), which causes krill to move above the hull-mounted echosounder and/or disperse into low-density aggregations. Additionally, because krill are relatively weak scatterers as compared to pollock, they can be 'shadowed' by pollock when both taxa co-occur (Coyle and Pinchuk 2002). This effect was estimated by calculating the proportion of cells occupied by pollock in a local region and applying a correction to the observed krill backscatter in this region based on the proportion of the 5 m × 5 ping analysis cells occupied by pollock (Ressler et al. 2012).

Finally, the historical method converted krill backscatter to density using a TS model developed for EBS krill (Smith et al. 2013). This model was applied to the krill length and species composition observed in catches from trawls targeted on acoustically-detected euphausiid aggregations, averaged over all surveyed years. Large, rare organisms were removed from the trawl catches, and the remaining mixture was sorted by the Polish Plankton Sorting and Identification Center (Szczecin, Poland) to provide species counts and identifications on a per-

trawl basis as well as up to 25 measured lengths per trawl for each observed species. Since this mixture was about 87% krill by number on average, all backscatter classified in the above manner was attributed to krill. Density was converted to biomass using empirical length-weight relationships (Harvey et al. 2012). Survey results have been reported as sums and averages of density and biomass for each year (Ressler et al. 2012, Hunt et al. 2016, Levine and Ressler 2024).

Updates to the historical method

The updated method retains the general steps summarized above and is best considered as a more general implementation and incremental improvement rather than a large-scale reconsideration. The rationale for, as well as the implementation and assessment of, updates to the historical method follows.

Acoustic data export and processing

In the historical method, the majority of the acoustic identification process was done with custom Echoview (various versions, Echoview Software Pty Ltd) and Matlab (various versions, The Mathworks, Inc.) routines. The Echoview routines produced exports of krill backscatter (s_A, m^2 nmi^{-2}) integrated at the EDSU level (i.e. 0.5 nmi horizontal × 20 m vertical resolution), while some Z-score thresholds and both the diel and shadow corrections were implemented using Matlab. In the updated method, cells are exported from Echoview at 5 ping horizontal × 5 m vertical resolution at all available frequencies, and corresponding noise measurements are similarly exported at each frequency. A total of 12 export types are now created: 5 S_v exports with no integration threshold applied (one per acoustic frequency for the 18, 38, 70, 120, and 200 kHz frequencies), 5 estimates of acoustic noise (S_v attributed to acoustic noise at each of the

above frequencies), and two exports with integration thresholds applied (120 kHz with a -80 dB re 1 m^{-1} threshold and 200 kHz with a -77.7 dB re 1 m^{-1} threshold). Echoview still functions in an important capacity in the updated method by providing an interface in which to apply acoustic calibration information, survey transect bounds, and user-corrected near-surface and near-bottom lines to remove artifacts from the acoustic data. However, we chose to move the remaining processing steps outside of Echoview to increase the flexibility and transparency of acoustic identifications. While these steps are currently accomplished using scripts written in R (version 4.5.0, R Core Team 2025), this flexibility allows other users to more easily use, evaluate, and modify our method for use in other applications or in other programming languages. As with the historical method, the final product of the updated analysis is exports of krill backscatter at 0.5 nmi horizontal × 20 m vertical resolution; we now export both measures of areal backscattering (s_A, m^2 nmi^{-2}) and volume backscattering (S_v, dB re 1 m^{-1}) attributed to krill.

Additionally, while preparing previous surveys for analysis using the updated method, we corrected small issues in past surveys (for example, the 2016 survey used one of two available calibrations and the survey is updated here to use the average of both). These re-exported surveys are referred to as the 'new base' in the **Results and Discussion** below and they represent the starting point for all other additions. To assess differences between the new base and the historical method, we compared the mean survey-level krill backscatter (s_A) from each method (n = 12 surveys for this and all subsequent comparisons).

Improvements to acoustic data quantity and quality

Since the development of the historical method, a number of improvements to the availability and quality of acoustic data have occurred. A 70 kHz echosounder has been used since 2008,

allowing for the 4-frequency identification process to be expanded to 5 frequencies. Based on 70 kHz data collected from 13 trawl-verified EBS krill aggregations (De Robertis 2010, see their Figure 4); values are summarized in Table A1.1), krill observed at 70 kHz demonstrate relatively high S_v as compared to those observed at lower frequencies (i.e. 18 and 38 kHz) and relatively low S_v as compared to those observed at higher frequencies (i.e. 120 and 200 kHz). In contrast, pollock observed at 70 kHz are relatively 'flat' in comparison to observations at lower and higher frequencies. Therefore, the addition of the 70 kHz acoustic data adds another meaningful acoustic contrast for use in multifrequency comparisons. We assessed the relative change in survey-scale backscatter for the updated 5-frequency identification process in comparison to survey-scale backscatter obtained via the 4-frequency historical method.

Acoustic species identifications can be compromised by background noise (i.e. the portion of the acoustic measurement that is from sources other than the backscattered transmitted sound; Simmonds and MacLennan 2005) that can mask the presence of sound scattering animals. This can be especially problematic with multi-frequency identification of relatively weak scatterers such as krill (Korneliussen 2000, De Robertis and Higginbottom 2007). Prior to 2024, noise was estimated from S_v measurements made during active pinging (De Robertis and Higginbottom 2007), which relied on the assumption that there was a portion of the active ping recording which was effectively 'signal-free' (i.e. dominated by noise). If this assumption is not met, noise may be overestimated. Starting in 2024, we intersperse background noise measurement ("passive pings") at a ratio of 1:9 passive:active pings. Because these interspersed passive noise measurements contain no active signal, the new method relies on fewer assumptions than the active method. Collecting more accurate measurements of background noise at each frequency will allow for unbiased multifrequency S_v comparisons (Korneliussen 2000).

Mitigating for changes in acoustic data quality over time

In addition to changing the noise estimation methodology for surveys from 2024 forward, we reassessed the noise estimation criteria used in previous surveys. The historical method did not assess background noise at 38 kHz (as assessed by passive noise measurements and visual inspection of echograms, the assumption that this frequency was effectively 'noise-free' for this application was supported at the time the historical method was developed). However, we have since experienced intermittent radiated vessel noise issues that can result in 38 kHz background noise estimates ~10 dB re 1 m^{-1} higher than those observed historically (McGowan et al. 2025). We therefore decided to assess noise at 38 kHz for the entire krill time series (with this addition, noise estimates are now made at all acoustic frequencies).

Similarly, the historical method required a SNR of ≥ 10 dB at all assessed frequencies. This threshold was used to develop the frequency response libraries underlying the Z-score multifrequency method (De Robertis et al. 2010) and was set conservatively to minimize the probability of noise biasing identification criteria. In developing the updated method, we explored less conservative SNR thresholds (0, 3, and 6 dB) as well as mixed approaches where higher thresholds (10 dB) were required at the frequency used for echo integration and lower thresholds (6 dB) at frequencies used only in multifrequency identification. The effects of applying different SNR thresholds were assessed as the difference in mean survey-scale krill backscatter from that obtained using the historical method (i.e. 10 dB at all frequencies except 38 kHz).

We have additionally encountered cases where valid (i.e. high SNR) 200 kHz observations are present in a given cell, but 120 kHz observations are not. In the historical method, valid S_v

measurements were required at 120 kHz for a cell to be classified as krill. In the updated method, we allow for cases where the 120 kHz value is not available (generally because it demonstrates SNR ≥ the SNR threshold value, equipment malfunctions, or is from platforms with fewer frequencies) but the 200 kHz is available. For example, the 2020 survey was conducted with a dual frequency 38/200 kHz echosounder on a USV which relied on this adjustment (Levine and De Robertis, 2025). Cells identified as krill in these cases are echo integrated as "120 kHz equivalent" by converting the observed 200 kHz backscatter to the expected 120 kHz backscatter based on the empirically-observed difference for krill backscatter at 120 vs 200 kHz ($S_{V,120kHz\ equivalent} = S_{V,200kHz}$-2.3) and applying a -77.7 dB re 1 m^{-1} integration threshold (see Levine and De Robertis, 2025 for details). We assess the effect of this addition as the difference in mean survey-scale krill backscatter from that obtained using the historical method (i.e. requiring a 120 kHz measurement for a measurement to be classified as krill).

Shadow correction

In the historical method, the correction for pollock 'shadowing' krill backscatter was applied at a different resolution than the resolution used for making acoustic identifications. When 5 m vertical × 5 ping horizontal grid cells were identified as pollock, the correction for the cells was calculated using the number of acoustic samples above the integration threshold (-80 dB re 1 m^{-1}) within the cells. This can lead to a persistent underestimate in shadow estimation in the historical method when pollock do not occupy an entire cell. For example, in a case where 100 grid cells (with each grid cell comprising 80 acoustic samples for a total of 8,000 samples) were used to determine local pollock overlap and 10 grid cells were identified as containing pollock above the integration threshold (comprising 450 samples because each grid cell was not entirely occupied by pollock) the correction factor would be calculated as:

$$1 + \frac{samples\ identified\ as\ pollock}{samples\ total}. \quad (Eq. 1)$$

Because each grid cell is unlikely to be 100% occupied by pollock samples above the integration threshold (i.e. no empty space), the correction factor can be different than if each grid cell was assigned to 'pollock' or 'non-pollock' in its entirety as is the case in the Z-score method (the correction factor would be 1 + (450/8000) = 1.06 in our above example case). In contrast, in the updated method a given cell can only be '100% pollock' or '100% non-pollock' for the shadow correction (all acoustic samples within a cell identified as pollock are assigned as pollock). In other words, the resolution at which cells are identified in the Z-score method matches the resolution at which the correction is calculated:

$$1 + \frac{grid\ cells\ identified\ as\ pollock}{grid\ cells\ total}. \quad (Eq. 2)$$

In our example case, the correction factor would be calculated as 1.10 (1 + 800/8000).

Index standardization

Over the 20-year EBS survey time series, the physical extent of surveys has varied. While surveys have always encompassed the middle (50 to 100 m) and outer (100 to 200 m) domains of the U.S. portion of the Eastern Bering Sea shelf (i.e. the 'core survey area'), they occasionally extend into the Russian portion of the shelf as well as areas to the north and east of St. Matthew Island (Stienessen et al. 2025). The historical method did not account for this variation, and included all observations made within a survey (inside and outside of the core survey area) when computing annual index values. In the updated method, we instead only include observations made within the core survey area so that the survey domain remains consistent throughout the

time series. To assess the impact of this update, we compare backscatter estimates that encompass all surveyed areas with those limited to the core survey area.

Removing marginal krill classifications

As noted above, the historical method removed marginal krill identifications by requiring krill to have a mean Z-score ≤ 1.5 in 20 m depth layers at the EDSU level. This acted as a statistical check on krill identifications, excluding krill from EDSUs with mean identifications ≥ 1.5 standard deviations (S.D.) more than those expected for krill. In the updated method, we instead use behaviorally-informed criteria. Ressler (2012) noted that EBS krill tend to be found in layers formed at least in part due to active swimming behavior, which suggests that krill cells are unlikely to be found in isolation. In the updated method, we require identified krill cells to be co-located with other krill cells by using the "Queen's case" contiguity rule, which required that ≥ 2 krill cell sides or corners touch another krill cell for a cell to be identified as krill (Levine and De Robertis 2025). We assess the impact of this criterion by calculating the change in backscatter resulting from its implementation as compared to backscatter obtained using the historical Z-score criteria.

Using krill catch data

As previously noted, estimates of krill length obtained from catch data strongly affect estimates of krill TS. The historical method assumed that krill lengths differed between shallower (< 100 m, "inshore") and deeper (> 100 m, "offshore") krill catches. This was based on observed differences in species and size composition, with slightly longer *T. inermis* primarily found in deeper strata and slightly shorter *T. raschii* found in shallower strata (Ressler et al. 2012). The historical method obtained two TS estimates (one for each depth strata) based on this

assumption. Additionally, the historical method estimated mean krill length in each stratum based on all available catch data averaged across sampled years. Given the catch record now extends over 20 years, we re-examined these practices in the updated method. Specifically, we examined patterns in krill length between shallow and deep strata, and we examined inter-annual variability in krill length estimates. We assessed the impact of removing the shallow and deep strata on annual mean length estimates, and we also assessed the impact of annual length estimation (as opposed to long-term mean length estimation) on survey-scale krill density estimates.

Converting backscatter to density and biomass

Since the development of the historical method, additional measurements of material properties, *in situ* tilt, and krill body shape in EBS krill species (*T. inermis*, *T. spinifera*, and *T. raschii*) have been conducted (Lucca et al. 2021, 2023). We incorporate this work into the updated method. In brief, we simulated 10,000 realizations of TS-at-length using draws from distributions of measured EBS density (g) and sound speed (h) contrasts, *in situ* krill orientation, krill body shape, and the TS offset (G_{ATS}, which represents the t-distribution of observed differences in krill TS when comparing modeled predictions and empirical measurements at 120 kHz; Lucca et al., 2023). We then calculated the mean TS-at-length in 1 mm increments from the 10,000 realizations to create a TS-length table for the range of krill we encounter in the EBS (5-35 mm as measured from the posterior of the eye to the tip of the telson). Although many of these measurements were collected on a per-species basis, our TS-length model is not species-specific, and instead combines measurements across species to produce a regionally-specific model. For details on the decision to parameterize a regionally- (but not species-) specific model, see ***Results and Discussion***. For details on parameters and model structure, see **Appendix II**.

Additionally, we determined a length-wet weight relationship based on previous measurements of *T. raschii*, *T. inermis*, and *T. longipes* in the EBS (Harvey et al. 2012). The EBS length-wet weight relationship was determined by fitting a linear regression to log-transformed krill length and wet weight measurements from Harvey et al. (2012), and back-transforming with a correction applied for the bias resulting from the back transformation (Miller 1984).

It is important to note that there are many different standards for determining the length of krill (Morris et al. 1988). We measured krill captured in targeted trawls from the posterior of the eye to the tip of the telson (Ressler et al. 2012), referred to here as "Poland length" to indicate the methodology of lengths measured by the Polish Plankton Sorting and Identification Center. We then group krill in 1 mm length bins defined at the center of each Poland length bin (i.e. krill measured at a Poland length of 18.0 to 18.9 mm are placed in the 18.5 mm bin). The updated TS-length model based on Lucca et al. (2021) defines length using 'standard length 2,' or the distance from the anterior of the eye to the posterior of the sixth abdominal segment (Mauchline 1980). We therefore parameterized our TS-at-length model using lengths converted from Poland length → standard length 2 based on published regressions from Poland length → standard length 1 (anterior of the eye to the posterior of the telson, Mauchline 1980) and from standard length 1 → standard length 2:

$$Poland\ length \rightarrow standard\ length\ 1 = 1.07 \times Poland\ length + 0.1041 \quad \text{(Eq. 3)}$$

($r^2 = 0.96, n = 231$; Ressler et al. 2012).

$$standard\ length\ 1 \rightarrow standard\ length\ 2 = 0.82 \times standard\ length\ 1 + -0.20 \quad \text{(Eq. 4)}$$

($r^2 = 0.93, n = 273$; Lucca et al. 2021).

No length transformations were required for calculating length-wet weight relationships. For simplicity, a lookup table is provided which provides per-mm TS and wet weight values at

Poland length, standard length 1, and standard length 2 equivalents (https://github.com/noaa-afsc-mace/KrillCommunication; also presented in Table A1.2).

Annual estimates of krill length and wet weight

The updated method calculates annual estimates of krill mean TS and wet weight based on krill catches within each survey year. Specifically, the amount of backscatter and biomass for an individual 'average' krill in each survey year *y* is calculated based on krill proportion-at-length in 1 mm length class increments *l*:

$$P_{,yl}=\frac{n_{,yl}}{\sum n_{,yl}}. \quad (\text{Eq. } 5)$$

TS-at-length is then converted to its linear equivalent, the backscattering cross-section σ_{bs}:

$$\sigma_{bs,l}=10^{\frac{TS_{,l}}{10}}\ (m^2). \quad (Eq. 6)$$

The average σ_{bs} for year *y*, $\hat{\sigma}_{bs,y}$, is then calculated as:

$$\hat{\sigma}_{bs,y}=\sum_{l=1}^{n}\sigma_{bs,l}\times P_{,yl}\ \ (m^2). \quad (Eq. 7)$$

Similarly, the average wet weight for year *y*, $\widehat{ww}_{,y}$, is calculated as:

$$\widehat{ww}_{,y}=\sum_{l=1}^{n} ww_{,l}\times P_{,ly}\ \ (mg). \quad (Eq. 8)$$

The terms $\hat{\sigma}_{bs,y}$ and $\widehat{ww}_{,y}$ can be thought of as the amount of backscatter and biomass for an average krill in year *y*.

Calculating density and biomass

The updated method yields krill acoustic backscatter in 0.5 nmi horizontal × 20 m vertical EDSUs in volume scattering (S_v, dB re 1 m^{-1}) and area scattering (s_A, m^2 nmi^{-2}) terms. Krill volumetric density for each EDSU *i* and depth bin *j* for year *y* is calculated by first converting $S_{v,ijy}$ to its linear equivalent $s_{v,ijy}$:

$$s_{v,ijy}=10^{S_{v,ijy}/10}(m^{-1}) \quad (Eq.9)$$

and dividing by $\hat{\sigma}_{bs,y}$:

$$krill\ volumetric\ density_{,ijy}=\frac{s_{v,ijy}}{\hat{\sigma}_{bs,y}}\ (m^{-3}). \quad (Eq.10)$$

Krill areal density is calculated by first converting s_A to the area backscattering coefficient s_a (this simply scales backscatter on a per m^2 basis as opposed to a per nmi^2 basis and also includes a factor of 4π):

$$s_{a,ijy}=\frac{s_{A,ijy}}{4\times\pi\times1852^2}\ (m^2m^{-2}) \quad (Eq.11)$$

and dividing by $\hat{\sigma}_{bs,y}$:

$$krill\ areal\ density_{,ijy}=\frac{s_{a,ijy}}{\hat{\sigma}_{bs,y}}\ (m^{-2}). \quad (Eq.12)$$

Krill areal density is then converted to biomass density using $\widehat{ww}_{,y}$:

$$krill\ biomass\ density_{,ijy}=\frac{krill\ areal\ density_{,ijy}\times\widehat{ww}_{,y}}{1000}\ (g\ m^{-2}). \quad (Eq.13)$$

Results and Discussion

SNR

Krill backscatter estimates were not highly sensitive to the choice of SNR threshold values used in the analysis. When the 12-survey time series was calculated using lower SNR threshold values (excluding cells with SNR ≤ 6 dB, as opposed to the historical method threshold of ≤ 10 dB), there was more variability in relation to the historical method, but survey mean values did not change greatly (Figure A1.1). At higher thresholds (excluding cells with SNR ≤ 10 dB or a mixed approach in which a 6 dB threshold was required at non-integration frequencies and a 10 dB threshold was required at integration frequencies), results were less variable in comparison to the historical method (Figure A1.1, note comparatively narrow distributions). The mixed 6 dB/10 dB approach was selected for future work as it balances high SNR for integration and lower SNR thresholds for species identification which is less sensitive to small amounts of noise. Values for the 6 dB/10 dB SNR thresholding method differed by 1.1% (-2.1% to 6.9% from the historical approach; all values are presented as mean and range over the 12-survey time series; Figure A1.1, Table 1).

In addition to changing SNR threshold values, the updated method assessed SNR at all measured acoustic frequencies, rather than only at 120 and 200 kHz. While this additional improvement from the historical method did not change estimates in the current time series, it can continue to act as a quality control step in future surveys. In a survey where unexpected noise issues arise on a previously unassessed frequency (for example, elevated 18 and 38 kHz noise due to vessel radiated noise; Bassett et al. 2024, McGowan et al. 2025) the SNR thresholds at all frequencies

in the updated method will explicitly prevent biased acoustic information from being included in multifrequency comparisons.

Acoustic krill identification

Although our updates to acoustic krill identification resulted in relatively minor impacts at the survey level (Figure 1), the following three updates had the most influence: the addition of the 70 kHz channel, the updated shadow correction, and the creation of 'new base' survey datasets (Figure 1).

The addition of the 70 kHz channel (allowing for 5-frequency multifrequency identification) reduced backscatter estimates from the 4-frequency baseline (-11.0% [-22.6% to -5.1%]; Figure 1, Figure A1.2, Table 1). As previously noted, measurements of krill backscatter at 70 kHz are higher than those made at 18 and 38 kHz, while measurements of pollock remain consistent at these frequencies (De Robertis et al. 2010; Table A1.1). Therefore, the addition of the 70 kHz channel provides more information in the acoustic range at which krill demonstrate strong frequency dependence. In the updated method, this additional contrast to the multifrequency identification process provided for more selective krill identifications, as indicated by the reduction in krill backscatter as compared to the 4-frequency identifications. This is consistent with previous work on krill multifrequency identification, which generally found that an increase in the number of frequencies used in identifications produces lower estimates (Jarvis et al. 2010, Simonsen et al. 2016, Levine and De Robertis 2025).

The impact of the shadow correction was similar in magnitude, but it increased backscatter estimates as compared to non-shadow corrected estimates (9.8% [4.9% to 16.4%]; Figure 1, Figure A1.2, Table 1). It is important to note that this correction is relatively large in comparison

to the shadow correction applied in the historical method (1.4% [0.5% to 4.2%] in surveys from 2004 to 2010; Ressler et al. 2012). However, as noted above, the historical method correction was biased low due to a mismatch in resolution between the acoustic identifications (5 ping horizontal × 5 m vertical cells) and the correction calculation (fine-scale acoustic samples), which resulted in the shadowing effect being underestimated. In the updated method, the resolution at which cells are identified matches the resolution at which the correction is calculated (all calculations are done at the 5 ping horizontal × 5 m vertical cell scale). Because the updated method only differs from the historical method in this modification, the higher estimates are expected.

The 'new base' survey datasets varied slightly from the previously published values (-1.9% [-12.7% to 4.3%]; Figure 1, Figure A1.2, Table 1). This was largely driven by one year in which the updated method made changes to processing methodology: in 2016, only a partial calibration had been applied in the published dataset. When 2016 was excluded, the new base values are more directly comparable to previously published values (-0.9% [-3.5% to 4.3%]). These smaller-scale changes are likely due to a change in cell geometry between the historical Echoview template file and the updated Echoview template file. In the historical Echoview template, the vertical extent of cells was defined by their range from the transducer face (generally located at 9.15 m below the surface). In the updated template, the vertical extend is instead defined by depth from the water surface (0 m). This leads to cells being defined at slightly different vertical positions in the water column in each method, which results in slightly different mean S_v within cells as the underlying acoustic sample set differs in each case.

The remaining changes to the acoustic processing only resulted in minor changes at the survey scale. Allowing for the 200 kHz measurement to 'fill in' for the 120 kHz measurement for echo

integration in cases where the 120 kHz was not available had very minor effects on the estimate (0.3% [0.0% to 1.8%]; Figure 1, Figure A1.2, Table 1). However, this addition is valuable in surveys where the 120 kHz measurements (but not the 200 kHz measurements) are impacted by background noise as it allows for taxa identifications to be made in cells where they would otherwise be lost.

Finally, the switch from using a statistical (mean Z-score in 0.5 nmi × 20 m EDSU) approach to a behaviorally-informed approach to removing isolated krill detections (requiring 2 neighbors for each identified krill cell) did not have a large impact on estimates (-1.7% [-5.5% to 1.7%]; Figure 1, Figure A1.2, Table 1). We explored the effect of the "Queen's case" neighbors requirement, requiring cells identified as krill to have between 0 and 3 neighbors to be retained as krill (Figure A1.3). We selected a requirement for 2 neighbors based on its similarity to the Z-score approach as well as its consistency with previous work utilizing the 2 neighbors criterion (Levine and De Robertis 2025). Overall, the contiguity criterion is well supported by survey observations that krill form spatially cohesive layers in the EBS during daytime (Ressler et al. 2012) and are therefore unlikely to be found in lone cells.

Backscatter distribution and abundance

The updated multifrequency identification method included 6 modifications to the historical method (Figure 1, Table 1). Some of these modifications decreased the observed total backscatter (i.e. the addition of 70 kHz data), while others increased it (i.e. the updated shadow correction) or showed slight and variable effects. Given this complexity, it is informative to compare the spatial and vertical distribution of krill backscatter from the updated method to that of the historical method. Annual patterns of distribution and abundance were very similar

between methods, with both high-abundance 'hotspots' and low-abundance areas captured similarly in the updated method (Figure A1.4). Estimates of center of gravity and inertia (geostatistical measures capturing the mean location and the dispersion of a population, respectively; Woillez et al. 2007) were also very similar between the historical method and the updated method in all survey years (Figure A1.5; center of gravity within 6.6 nmi [2.8 nmi to 14.0 nmi]; note that the survey area covers an extent of approximately 570 nmi length × 175 nmi width), further supporting the similarity of estimates made with each method. The mean depth of the observed krill backscatter over the survey time series (weighted by backscatter) was also similar between methods (Figure A1.6; historical method 98.5 m [82.7 m to 127.8 m]; updated method 96.8 m [83.1 m to 133.5 m], indicating that both methods identified the majority of the krill backscatter at a similar vertical location.

Index standardization

Limiting observations to the core survey area resulted in moderate differences on a per survey basis (-1.0% [-8.4% to 6.0%], Figure 1, Figure A1.2, Table 1). This was most evident in years where krill were abundant outside of the core survey area (for example, on the Russian shelf in 2014) or there was relatively sparse krill backscatter outside of the core survey area (for example, in shallow waters northeast of St. Matthew Island in 2018). Although the ability to track trends outside of the core survey area is complicated by the infrequent and sporadic nature of surveys of these regions, we concluded that the overall index is improved by removing the non-core areas as this increased the ease of interpretation over the time series.

Krill catch data

Targeted krill trawling effort varied substantially since 2004, with periods of relatively high effort (2007 to 2012, where 12+ trawls per year were conducted) and low effort (prior to 2007 and after 2012, where 1 to 8 trawls per year were conducted). While sampling from 2007 to 2012 consistently occurred over the extent of EBS shelf and consistently sampled backscatter 'hotspots,' sampling in earlier and more recent years was comparatively sparse and occasionally missed hotspots (compare Figure A1.7 and Figure A1.4).

Despite the patchy nature of this dataset, there are some spatially and temporally consistent trends in krill size. Larger krill tended to be observed on the southeastern EBS shelf south of the Pribilof Islands between the 50 m and 200 m isobaths (the consistent geographic center of the krill population; Figure A1.5) and smaller krill were more commonly observed in the northern portion of the EBS shelf (Figure A1.7). Although there were differences in mean krill size between inshore and offshore catches (one-way ANOVA, $p < 0.01$), differences in observed krill length were small (from 2004 to 2022, offshore krill were 0.14 mm larger on average than inshore krill) and inconsistent between inshore and offshore strata: in 5 of 10 years where trawls occurred in both strata, offshore krill were larger than inshore, while in the other 5 years inshore krill were larger. This is evident in the broad overlap between deeper and shallower strata (Figure A1.8a). Therefore, we decided to remove the 'inshore' and offshore' strata distinction used in the historical method. This had only a minor effect on krill length estimates: as compared to the historical division by strata, krill length declined by 0.7% [-4.5% to 6.5%] (Figure 1, Table 1).

Krill lengths did vary interannually (one-way ANOVA, $p < 0.01$), with a period of relatively short krill since 2016 in contrast to relatively long krill observed from 2004 to 2014 (Figure A1.8b). The range of observed mean krill lengths (~3.5 mm over the 2004 to 2024 dataset) is substantial given the length of EBS krill (~19 mm averaged over the time series). Because there were clear interannual trends in krill size despite our limited sampling, we decided to use the annual mean krill length to apply TS estimates from the krill TS model instead of a long-term mean length. This approach produced krill density estimates that differed substantially from the historical method (krill density changed by 22.3% [-30.6% to 96.8%] when using annual mean lengths; Figure 1, Table 1). In future surveys where trawl effort may be very minimal (<3 hauls), it may be appropriate to rely on trawls conducted in the previous survey to estimate krill lengths. Conversely, if future surveys can obtain more extensive krill biological samples, it may be possible to provide species- and size-structured estimates of krill density and biomass in the EBS.

In terms of species composition, previous research indicated that *T. inermis* was more common at bottom depths > 100 m and *T. raschii* is more common at depths < 100 m (Coyle and Pinchuk 2002, Pinchuk and Coyle 2008); our trawl samples collected 2004 to 2018 were consistent with this (Ressler et al. 2012, Levine and Ressler 2024). However, the relatively sparse sampling in each survey (particularly in recent years) did not allow for examination of spatial patterns in krill species composition in each survey. For the same reason, although previous measurements suggested there were species-level differences in wet weight at length (Harvey et al. 2012; replotted in Figure A1.9), we fit a single length-wet weight curve that combined all species-level measurements (*T. inermis*, *T. raschii*, and *T. longipes*). This is in keeping with the taxonomic resolution of our regionally- (but not species-) specific TS-length model (see *Krill TS*

parameterization below). This curve likely overestimates *T. raschii* wet weight-at-length and underestimates *T. inermis* wet weight-at-length, but provides a reasonable relationship for the krill group as a whole (Figure A1.9).

We re-examined the relative taxonomic composition of catches to confirm that trawls, which are targeted on layers of probable krill based on their appearance in acoustic echograms, have continued to predominantly capture krill throughout the entire sampling period. The overall net catch was numerically dominated by krill species (88% of total individuals from 2004 to 2024; Figure A1.10a). It is important to note that catch composition is not equal to acoustic contribution. For example, the second most commonly captured group in our trawls were copepods (*Neocalanus cristatus*; Figure A1.10a). These are comparatively weak acoustic scatterers at 120 kHz, with TS at a given length approximately 20 dB lower than that of krill (see Lavery et al. 2007, their Figure 1). Hyperiid amphipods, the third most abundant group (Figure A1.10a), likely have a similar TS at length to krill given their taxonomic similarity, but were comparatively small (14.1 cm mean ± 3.3 cm S.D., n = 31 measurements). Given the relatively low numeric contribution of non-krill taxa to the catch, as well as their relatively low acoustic contribution, it is reasonable to continue assuming that krill are the dominant acoustic target in this time series. In addition, most of the krill captured were *T. raschii* and *T. inermis* (Figure A1.10b), and there was no evidence of a clear change in krill species composition over time.

Krill TS parameterization

Although many of the parameters required for the updated TS model were measured on a species-specific basis (Lucca et al. 2021), we chose to parameterize a region-specific model that applies to all observed EBS krill species. This choice was primarily motivated by our relatively

low trawl sampling effort: because we did not have sufficient samples on an annual basis to confidently observe spatial patterns in krill species distribution (and, therefore, to assign observed krill backscatter to species groups), we decided it was not appropriate to use species-specific TS models. The updated TS-length relationship is presented in Figure A1.11. The broad simulated distributions at each 1 mm length bin (Figure A1.11a) indicate that the model is highly sensitive to input parameters, especially the krill radius of curvature ratio (ρ_c) and krill orientation in relation to the acoustic wave (θ; Lucca et al. 2021). Bimodal distributions of TS at length, which are especially evident at larger body sizes (Figure A1.11a), are primarily due to krill orientation. The simulation approach used in this study indicated that taking the mean TS at each 1 mm length class provided a reasonable estimate given the variation in TS from empirically-collected input parameter distributions (Lucca et al. 2021, 2023).

The updated TS model suggested that krill are substantially stronger scatterers at all length classes than predicted by the Smith et al. (2013) model used in the historical approach (Figure A1.11b). At the range of lengths observed in the 2004 to 2024 catch data (annual mean krill length 16.7 mm to 20.7 mm) this corresponded to a 4.5 dB to 6.9 dB increase in TS in the updated TS model as compared to the historical model (Figure A1.11b). The increase in TS led to a corresponding decrease in krill density: as compared to the historical method, krill density declined by 71.3% [-79.4% to -64.1%] (Figure 1, Table 1). For details on parameter distributions and model structure, see **Appendix II**.

Importance of krill length estimates in converting backscatter to biomass

Because krill TS is highly length-dependent (Figure A1.11), it is informative to estimate the magnitude of changes in density and biomass due to length over the lengths of krill observed in

the EBS. As previously noted, krill density is calculated by dividing krill backscatter by an estimate of the amount of backscatter that a single 'average' krill represents (see *Calculating density and biomass*, above). The average amount of backscatter from a single krill (i.e. $\hat{\sigma}_{bs}$) was highly size-dependent (Figure A1.12a), with a ~2-fold increase in σ_{bs} over the range of mean krill lengths observed from 2004 to 2024 (Figure A1.12b). This led to a strong size-dependence in the number of individuals (Figure A1.12c, A12d) and grams of wet weight (Figure A1.12e, A12f) per unit backscatter. At a mean length of 17.5 mm (similar to the 2016 to 2024 period; Figure A1.12b), a single unit of backscatter (s_A, m^2 nmi^{-2}) resulted in 14.6 individuals $nmi^{-2}/1$ s_A and 0.81 g $nmi^{-2}/1$ s_A; at a mean length of 20.5 cm (similar to the 2009 to 2012 period; Figure A1.12b), this resulted in 7.2 individuals $nmi^{-2}/1$ s_A and 0.67 g $nmi^{-2}/1$ s_A.

Summary: processing steps in the updated method

This section summarizes the steps in the revised method used to estimate krill density. Refer to the preceding sections for details on each step.

1) Echo integrate acoustic backscatter from the verified surface exclusion (16 m depth) to the bottom exclusion (0.5 m above the bottom detection) at each frequency at 5 ping horizontal × 5 m vertical resolution cells using appropriate integration thresholds. For use in acoustic krill identification ("dB-differencing"), integrate with no integration threshold. For use in integrating identified krill cells, echo integrate at 120 kHz with a -80 dB re 1 m^{-1} threshold and 200 kHz with a -77.7 dB re 1 m^{-1} threshold.

2) Remove all observations before local sunrise and after local sunset.

3) Remove all observations outside of the 'core survey area.'

4) Estimate noise for each cell via analysis of active (2004 to 2022) or passive pings (2024 onward) pings.

5) Calculate SNR at each frequency for each 5 ping × 5 m cell. Remove all data with SNR < 10 dB at the integration frequency and < 6 dB at other frequencies on a frequency specific basis.

6) Compute Z-score relative to krill, pollock, jellyfish and myctophid categories for all frequency pairs. Identify krill cells as those with Z-score relative to krill (Z_{krill}) of ≤ 2 and where Z_{krill} is the lowest of all categories.

7) Echo integrate krill cells into 0.5 nmi horizontal × 20 m vertical EDSUs by summing s_A by depth and averaging horizontally.

8) Apply shadow correction on 0.5 nmi horizontal × 20 m vertical EDSUs.

9) Compute euphausiid length distribution from all measurements in the survey year, pooling across species. If < 3 hauls are available, sequentially pool previous years until 3 hauls are available.

10) Convert from acoustic units to krill density and biomass by estimating the mean TS and wet weight of a 'representative' krill using updated TS-length and weight relationships (i.e. divide acoustic units by mean TS to obtain density estimates, and multiply density estimates by wet weight to obtain biomass estimates).

11) Obtain annual index estimates of the mean krill backscatter, density, and biomass.

Appendix I Tables and Figures

Table A1.1. ΔS_v values at 70 kHz for krill and pollock from De Robertis et al. (2010). The number of hauls refers to the number of trawl samples used to determine ΔS_v values. These data are reproduced here for reference as they are not presented in the tables in the original publication.

Taxon	N hauls	$\Delta S_{v,18-70}$	$\Delta S_{v,70-38}$	$\Delta S_{v,120-70}$	$S_{v,200-70}$
krill	13	-20.9 ± 1.7	9.0 ± 1.4	5.6 ± 1.4	7.6 ± 1.5
pollock	8	0.5 ± 3.2	-0.4 ± 2.3	-0.6 ± 1.6	-2.1 ± 2.2

Table A1.2. Target strength (TS, dB re 1 m^2) and wet weight-to-length lookup table. TS-length values are based on scattering model parameters from Lucca et al. (2021) as described in **Appendix II**; values are provided both as TS and its linear equivalent, σ_{bs} (m^2). Wet weight-length values are based on data collected by Harvey et al. (2012). Note that lengths are provided in 3 standard forms for convenience.

Poland length (mm)	SL1 length (mm)	SL2 length (mm)	σ_{bs} (m^2)	TS (dB re 1 m^2)	Wet weight (mg)
5.5	6.0	4.7	4.081E-12	-113.893	1.251
6.5	7.1	5.6	1.050E-11	-109.789	2.161
7.5	8.1	6.5	2.270E-11	-106.439	3.452
8.5	9.2	7.3	4.372E-11	-103.593	5.200
9.5	10.3	8.2	7.735E-11	-101.115	7.483
10.5	11.3	9.1	1.289E-10	-98.899	10.384
11.5	12.4	10.0	2.056E-10	-96.870	13.986
12.5	13.5	10.9	3.105E-10	-95.080	18.376
13.5	14.5	11.7	4.590E-10	-93.382	23.640
14.5	15.6	12.6	6.451E-10	-91.904	29.870
15.5	16.7	13.5	8.856E-10	-90.528	37.158
16.5	17.8	14.4	1.166E-09	-89.333	45.596
17.5	18.8	15.2	1.584E-09	-88.002	55.281
18.5	19.9	16.1	1.966E-09	-87.064	66.309
19.5	21.0	17.0	2.540E-09	-85.951	78.780
20.5	22.0	17.9	3.207E-09	-84.939	92.792
21.5	23.1	18.7	3.805E-09	-84.197	108.448
22.5	24.2	19.6	4.625E-09	-83.348	125.849
23.5	25.2	20.5	5.578E-09	-82.535	145.101
24.5	26.3	21.4	6.585E-09	-81.815	166.308
25.5	27.4	22.3	7.623E-09	-81.179	189.576
26.5	28.5	23.1	8.651E-09	-80.630	215.015
27.5	29.5	24.0	9.871E-09	-80.057	242.732
28.5	30.6	24.9	1.131E-08	-79.464	272.838
29.5	31.7	25.8	1.219E-08	-79.139	305.444
30.5	32.7	26.6	1.417E-08	-78.486	340.662
31.5	33.8	27.5	1.558E-08	-78.075	378.605
32.5	34.9	28.4	1.708E-08	-77.675	419.387
33.5	35.9	29.3	1.759E-08	-77.547	463.125
34.5	37.0	30.2	1.979E-08	-77.035	509.933
35.5	38.1	31.0	2.148E-08	-76.679	559.930

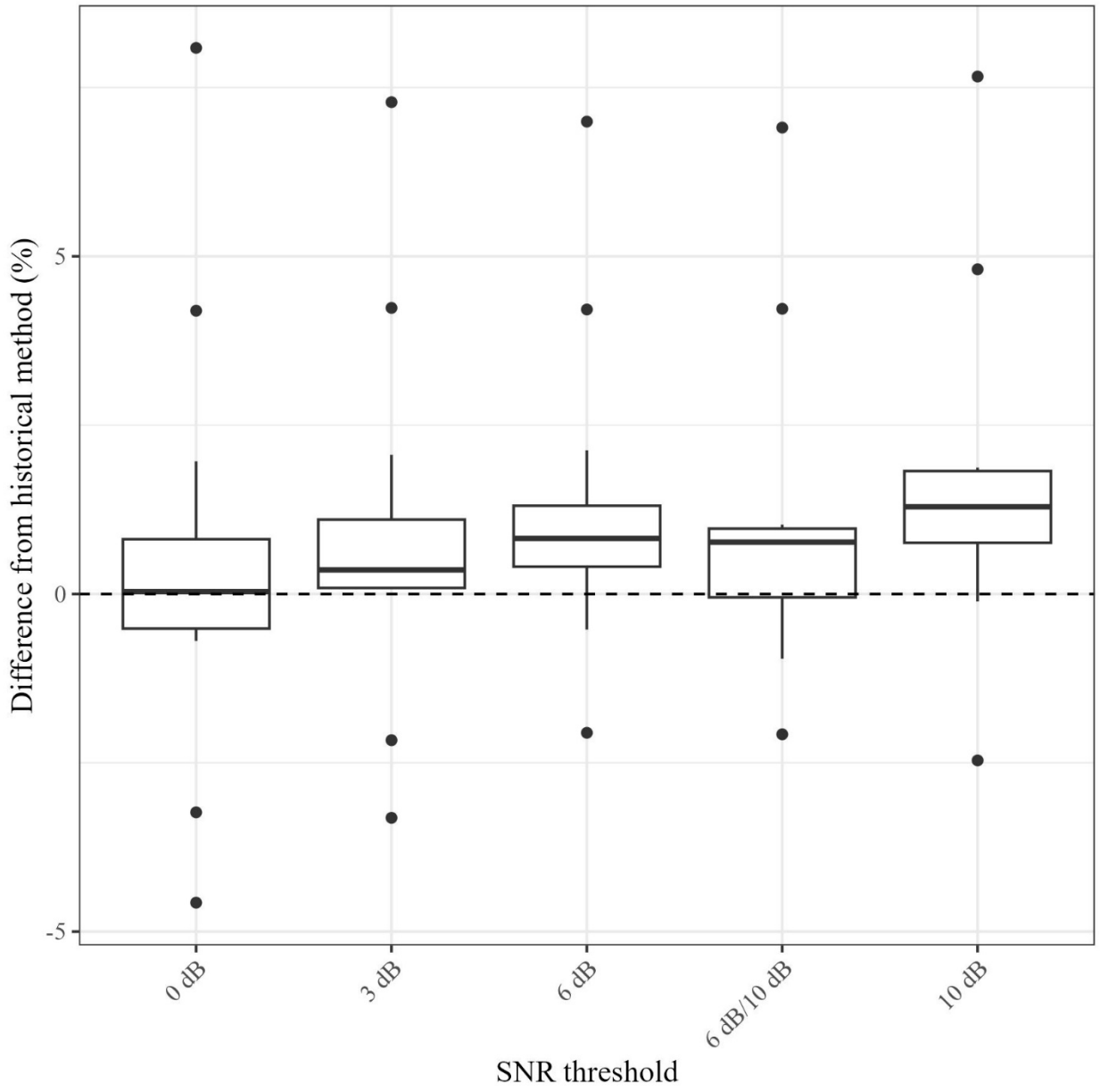


Figure A1.1. Effect of different SNR thresholds. Values are presented as the difference in mean krill backscatter from the historical method on a per-year basis (n = 12 years). The SNR threshold is defined as the minimum SNR required for a cell to be included in the krill identification process. “6 dB/10 dB” indicates a 6 dB SNR threshold at non-integration frequencies (18, 38, and 70 kHz) and a 10 dB threshold at integration frequencies (120 or 200 kHz). Note that the historical method excluded cells with SNR < 10 dB at 18, 120, or 200 kHz and did not assess SNR at 38 kHz; in the updated method SNR is assessed at all frequencies. The solid line within each boxplot represents the median difference from the initial method, the lower and upper limits of each box represent the first and third quartile, whiskers represent 1.5 times the interquartile range and dots represent outliers.

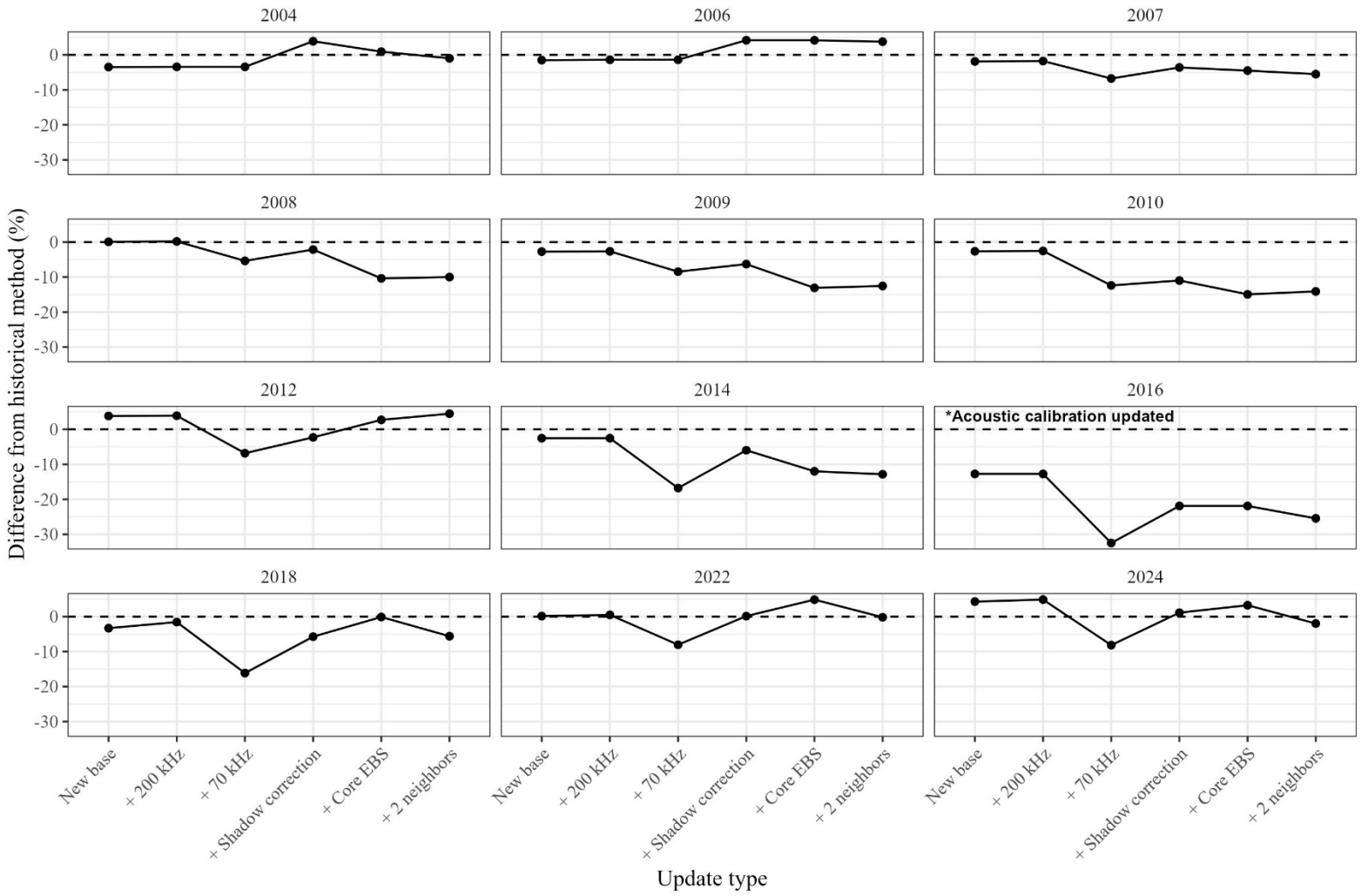


Figure A1.2. Effect of acoustic backscatter processing and index standardization updates on average annual krill density. Each update is added sequentially and includes all previous updates (i.e. '+2 neighbors' includes all additional updates while 'New base' includes no additional updates). See Table 1 for a summary of each update type.

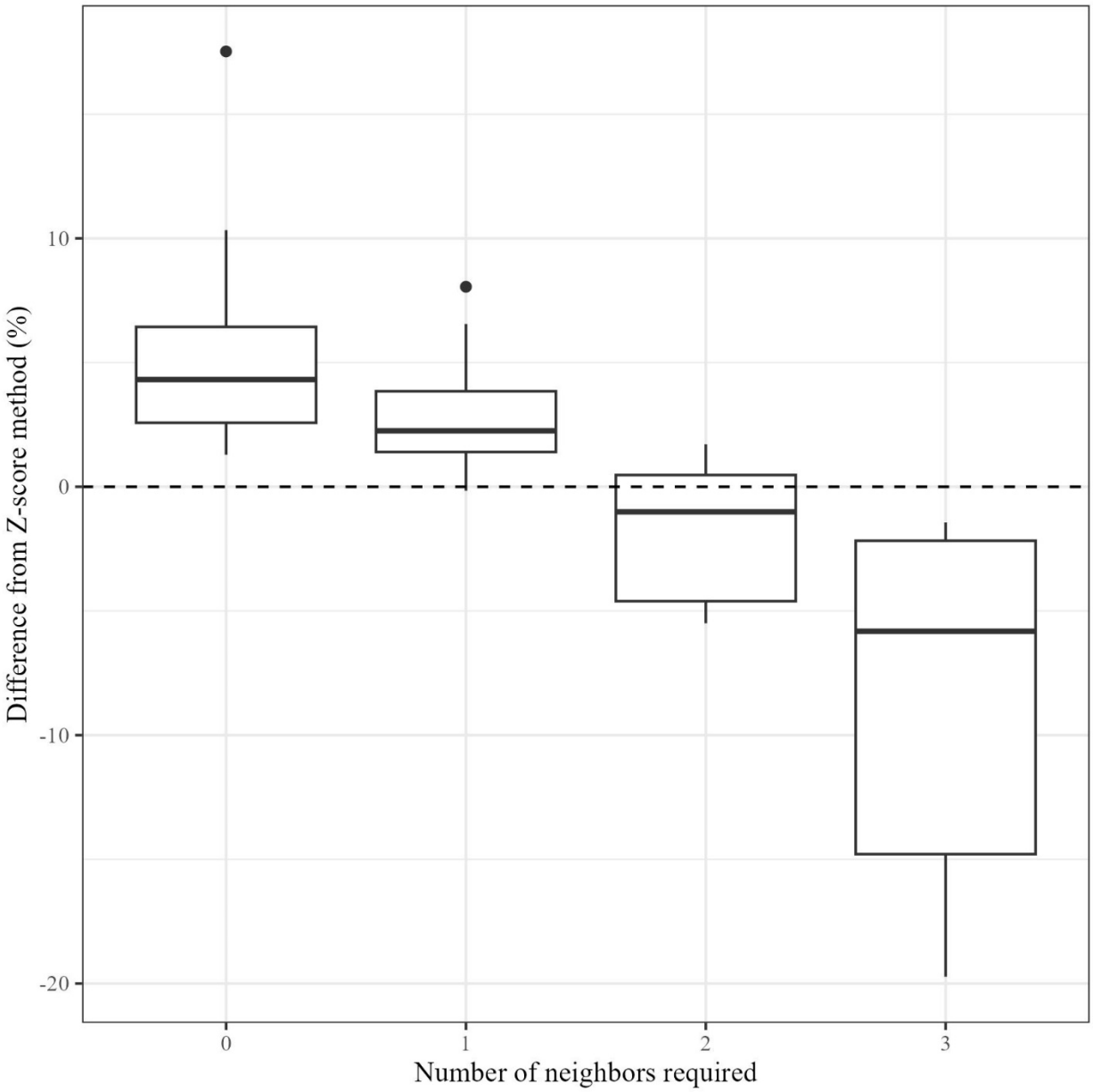


Figure A1.3. Effects of removing non-contiguous krill identifications. Values are presented as the difference in mean krill backscatter from the Z-score approach used in the historical method (n = 12 years). The solid line within each boxplot represents the median difference from the Z-score approach, the lower and upper limits of each box represent the first and third quartile, whiskers represent 1.5 times the interquartile range, and dots represent outliers.

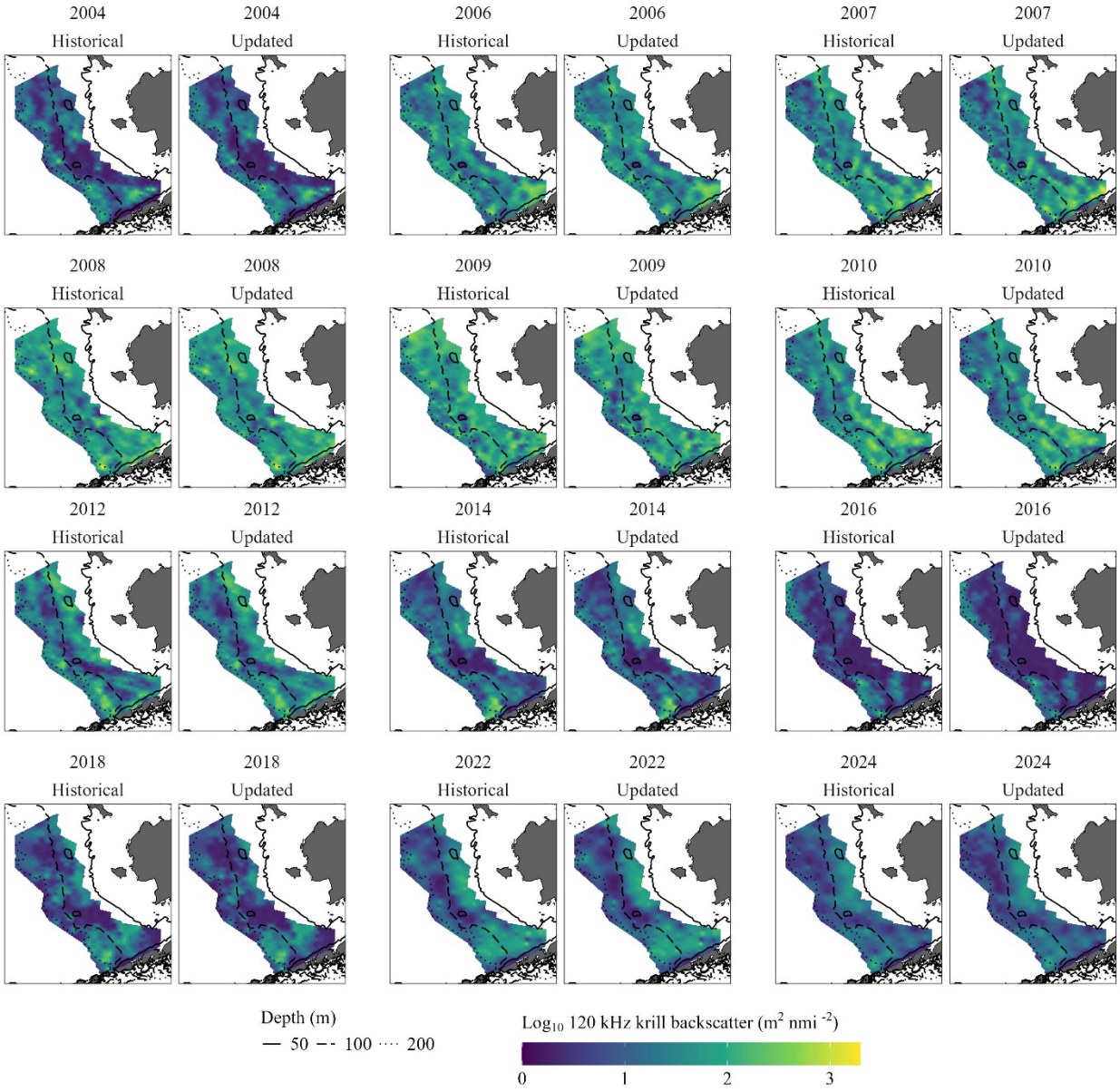


Figure A1.4. Time series of krill backscatter measurements for both the historical (left panels within each year) and updated methods (right panels within each year) methods. Values are interpolated using universal kriging (Pebesma, 2004) to make distributions easier to compare.

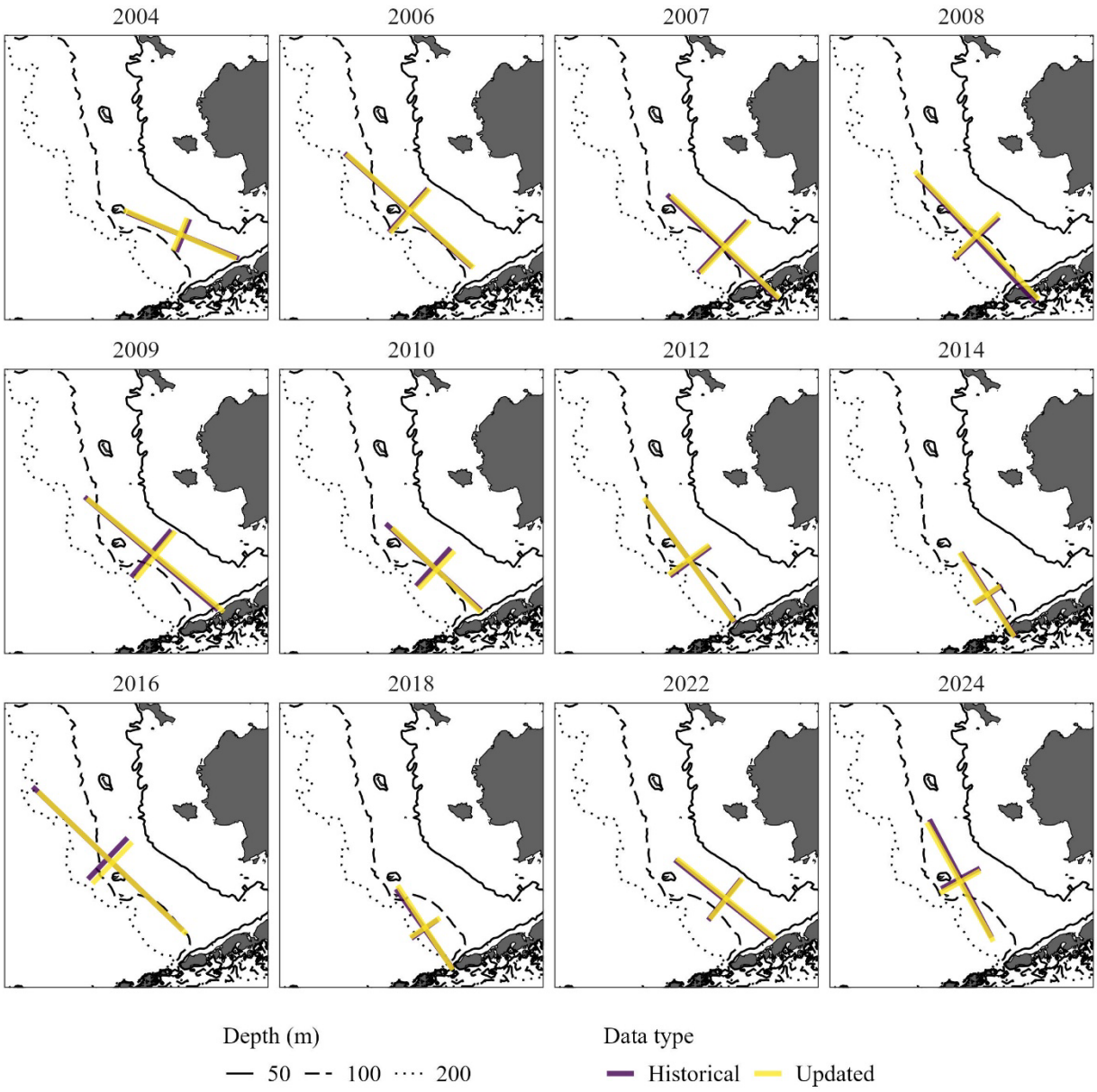


Figure A1.5. Center of gravity and inertia (geostatistical measures of the mean location of a population) of krill backscatter on an annual basis for both the historical and updated methods. The center of gravity is indicated by the intersection of crosses, while inertia is indicated by crosses.

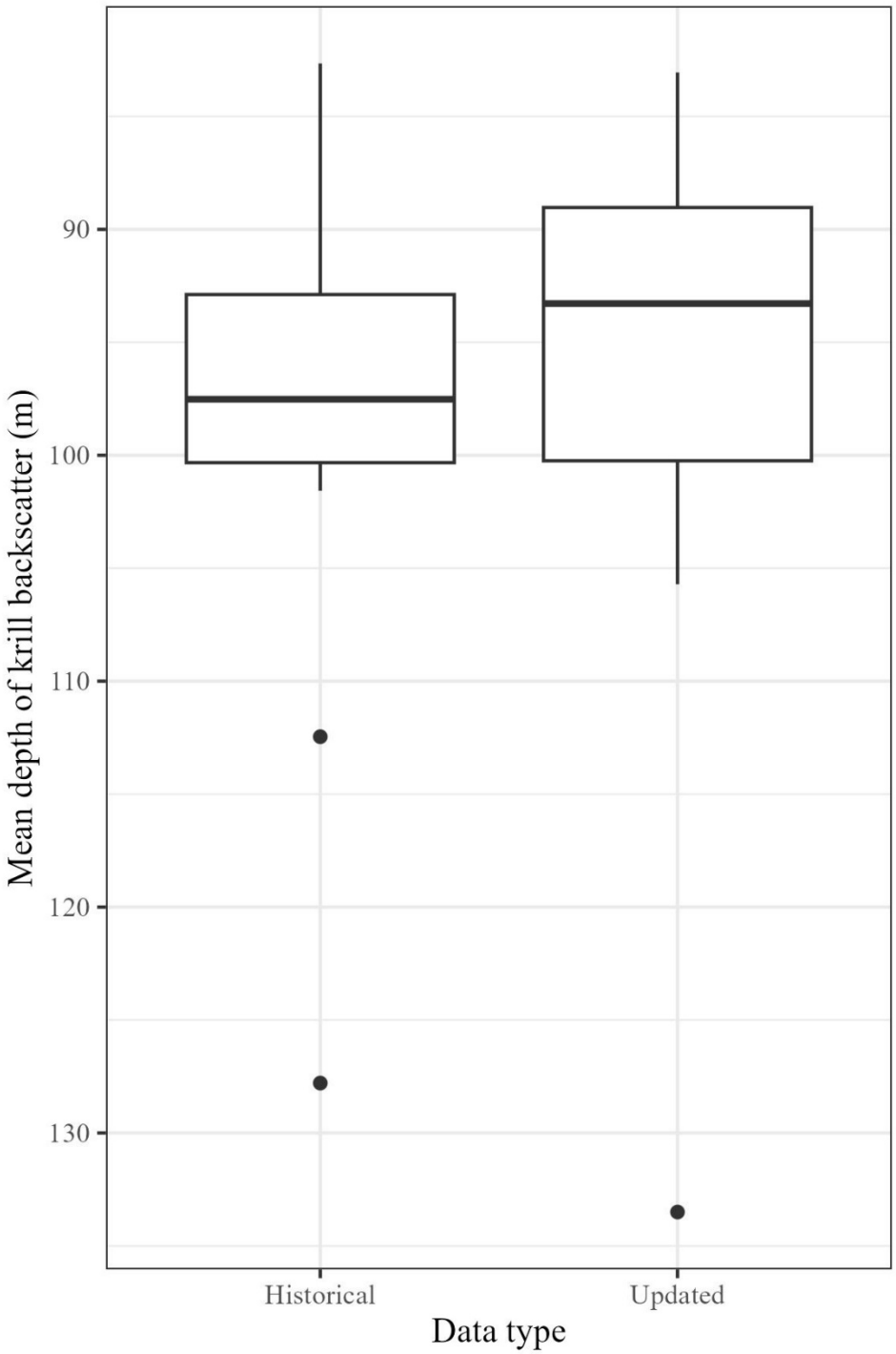


Figure A1.6. Mean depth of krill backscatter (weighted by abundance) for the historical and updated methods (n = 12 years). The solid line within each boxplot represents the median depth of krill backscatter, the lower and upper limits of each box represent the first and third quartile, whiskers represent 1.5 times the interquartile range, and dots represent outliers.

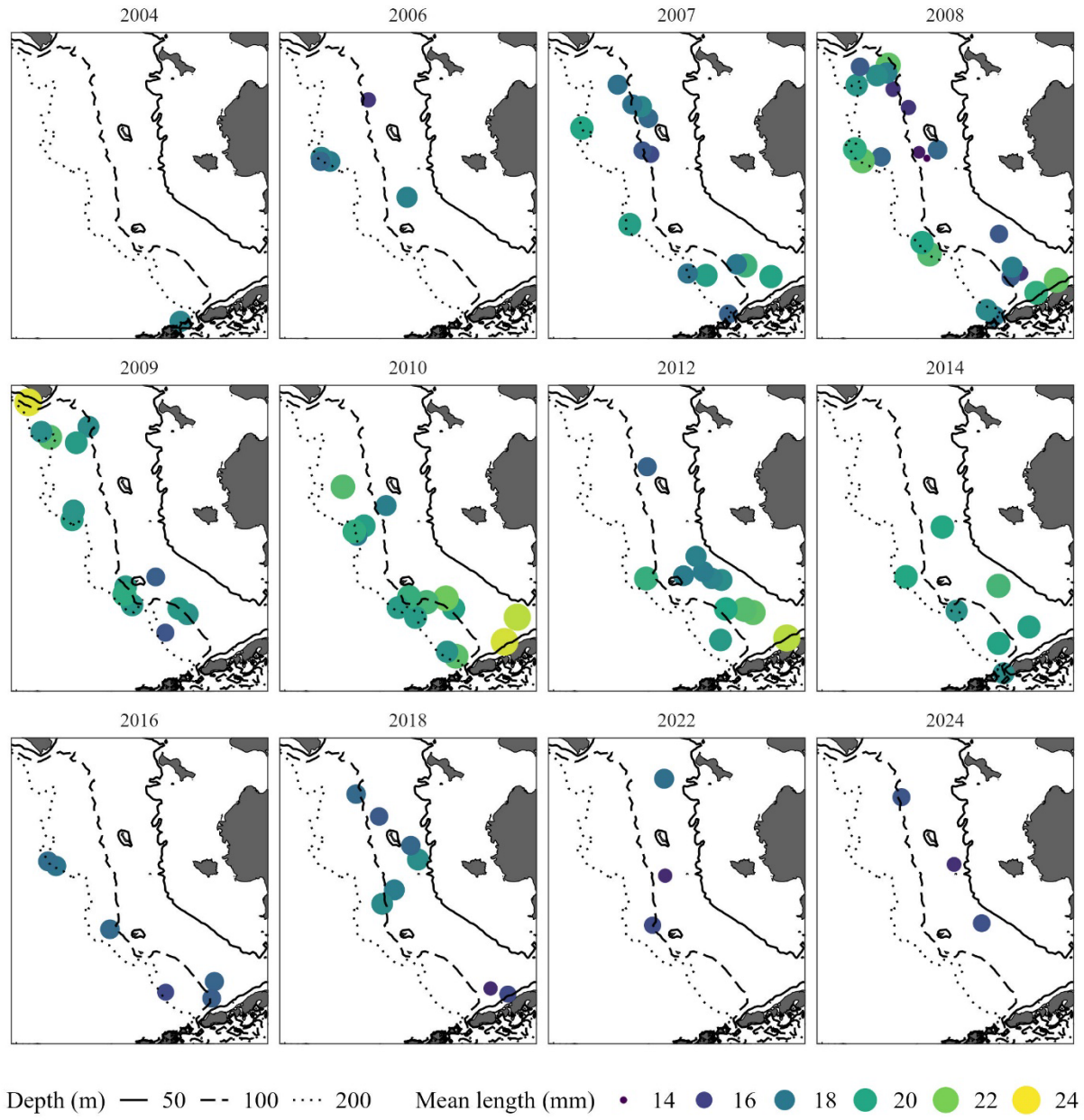


Figure A1.7. Krill catch data from Methot trawls from 2004 to 2024. Circles indicate trawl locations and are colored and sized by the mean length of krill captured in the trawl.

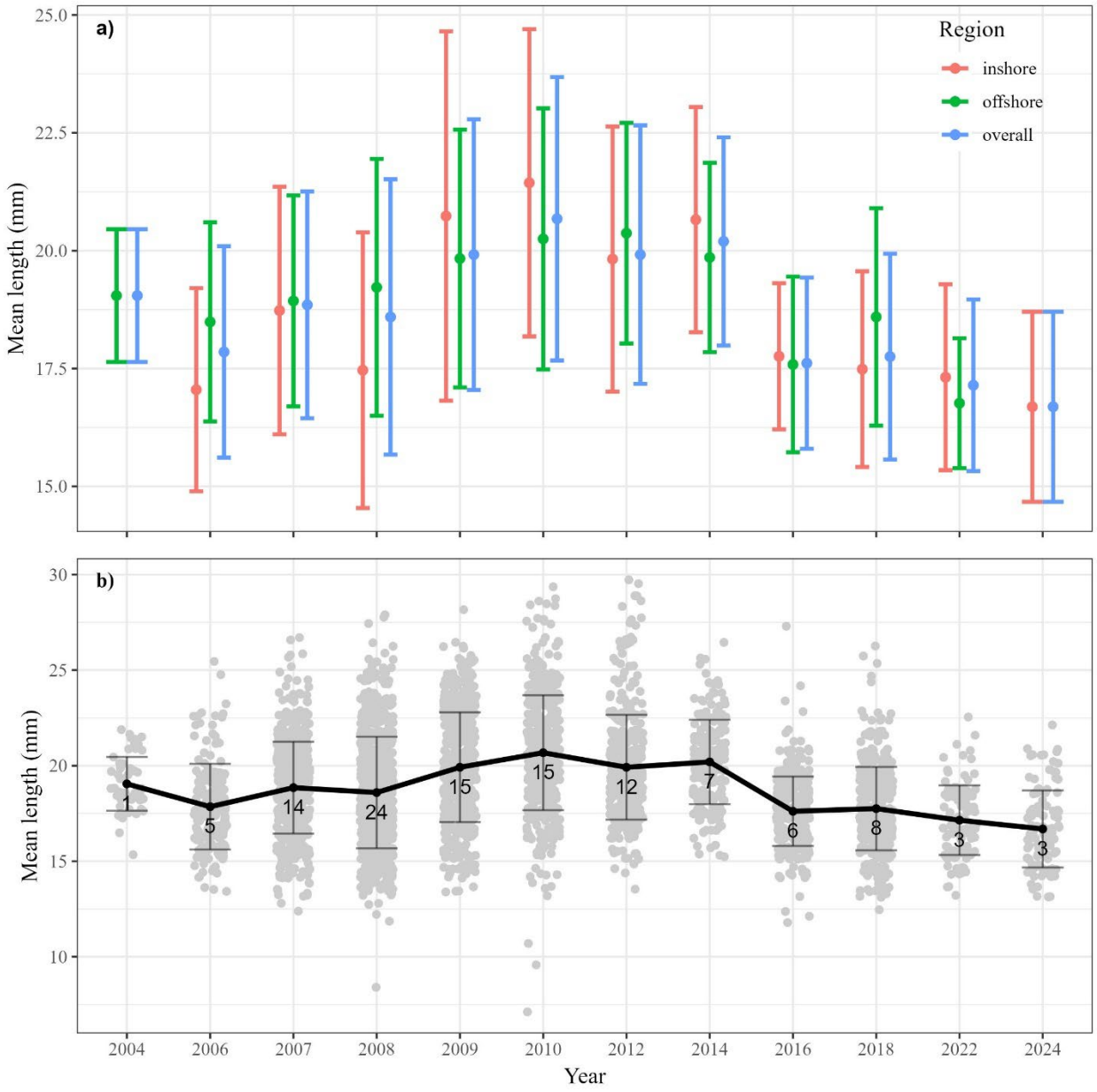


Figure A1.8. a) Mean krill length (+/- 1 S.D.) by year for the inshore (< 100 m bottom depth), offshore (≥ 100 m bottom depth) and overall (inshore and offshore combined) strata. b) Overall mean krill length (black points and line) as well as all measured krill lengths (grey points) and S.D. (black vertical whiskers) on a per-year basis. Number of trawls per year is noted below the annual mean.

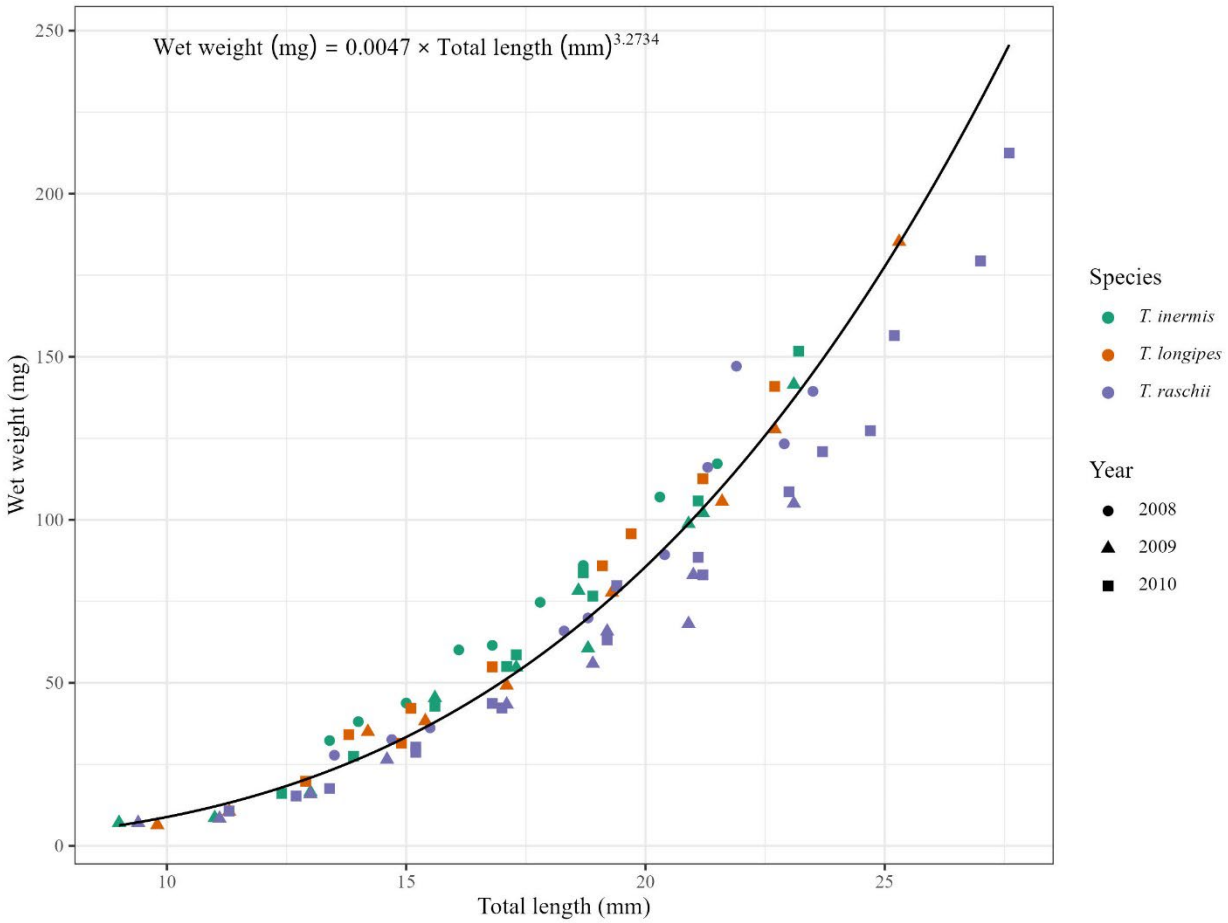


Figure A1.9. Krill total length-wet weight conversion. Data are from Harvey et al. (2012). Note that we use a single conversion (irrespective of species or year) but indicate species (color) and year (shape) to demonstrate inter-annual and inter-species variation in the length-weight relationship; a single model is used because annual estimates of species composition are likely to be unreliable given our low annual krill trawl sampling effort (see Figure A1.10 for sample sizes).

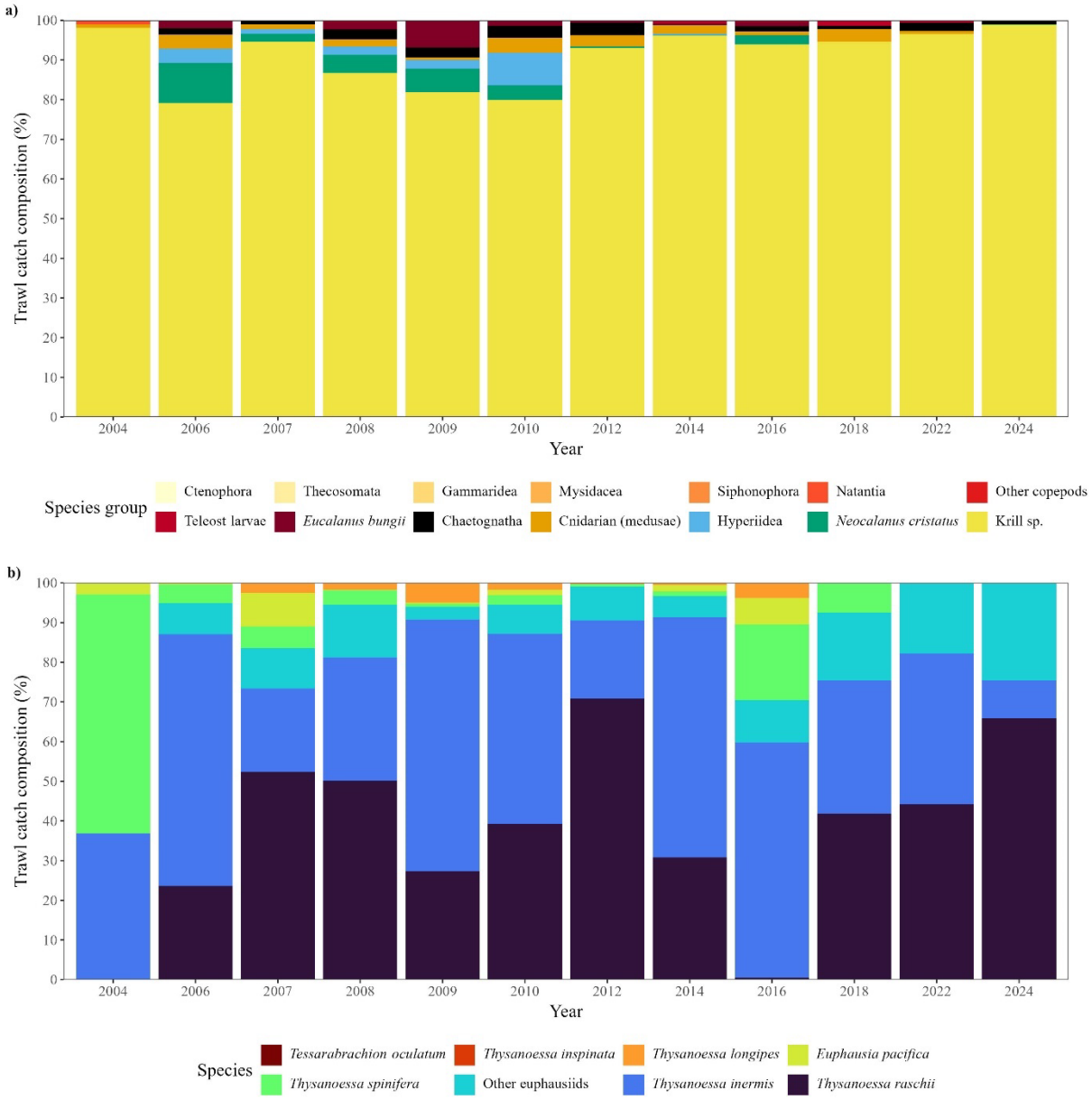


Figure A1.10. Trawl species composition from 2004 to 2024. a) Per-year catch composition by species group. All krill species are grouped into a single group (‘Krill sp.’). b) Per-year species composition within the grouped ‘Krill sp.’ category.

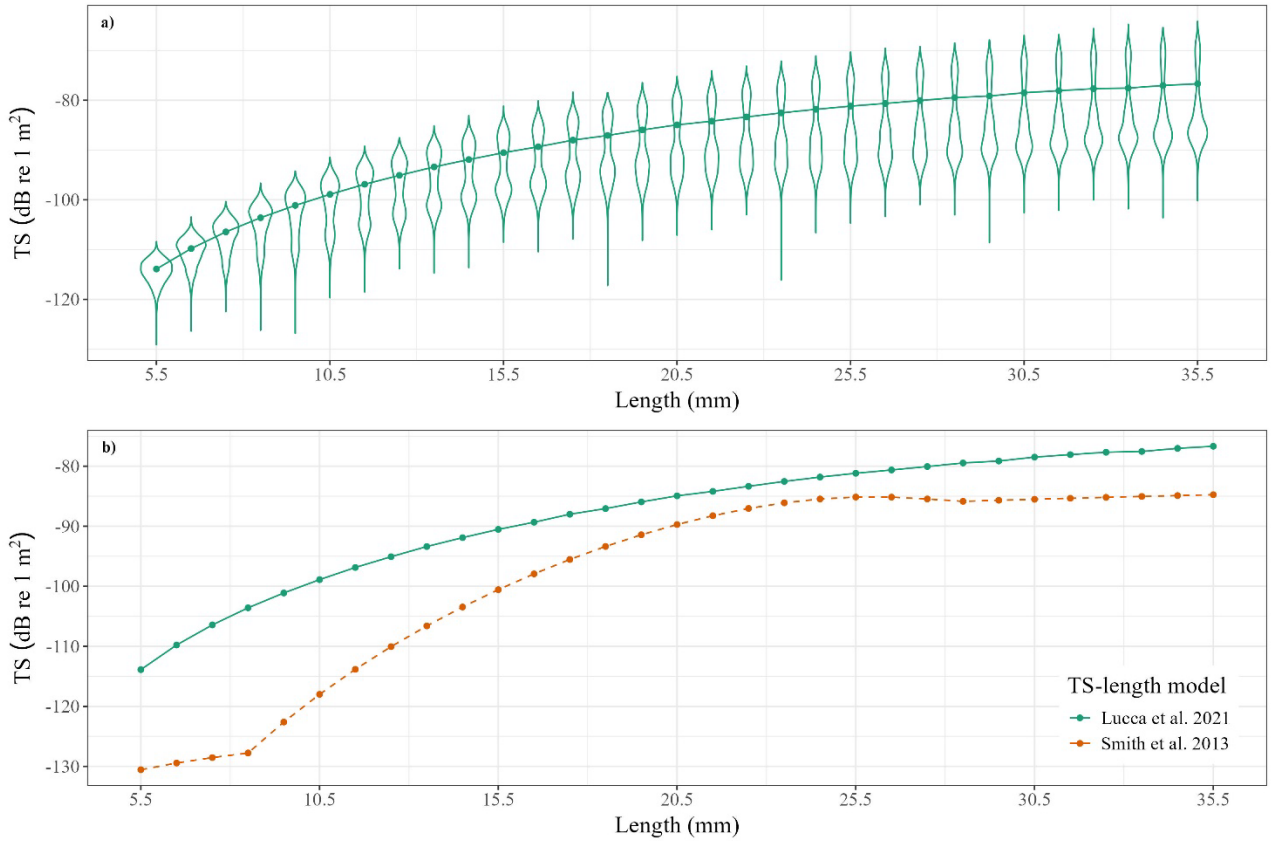


Figure A1.11. a) EBS krill target strength (TS)-length model (Lucca et al. 2021, 2023) used to convert 120 kHz krill backscatter to units of krill density in the updated method. Violin plots represent the kernel density estimates of TS at each length, based on 10,000 simulations drawn from specified distributions of material properties, radius of curvature ratio, and orientation (relative to the incident sound wave) for EBS-specific krill species (see Appendix 2). b) Comparisons of length-specific mean TS using parameters from Lucca et al. (2021; solid green line) and Smith et al. (2013; dashed orange line) that informed the updated and historical TS-length models, respectively. In both panels, points indicate TS estimates made at 1 mm intervals while lines are plotted to make trends easier to follow and are simply interpolations between the estimates made at 1 mm intervals.

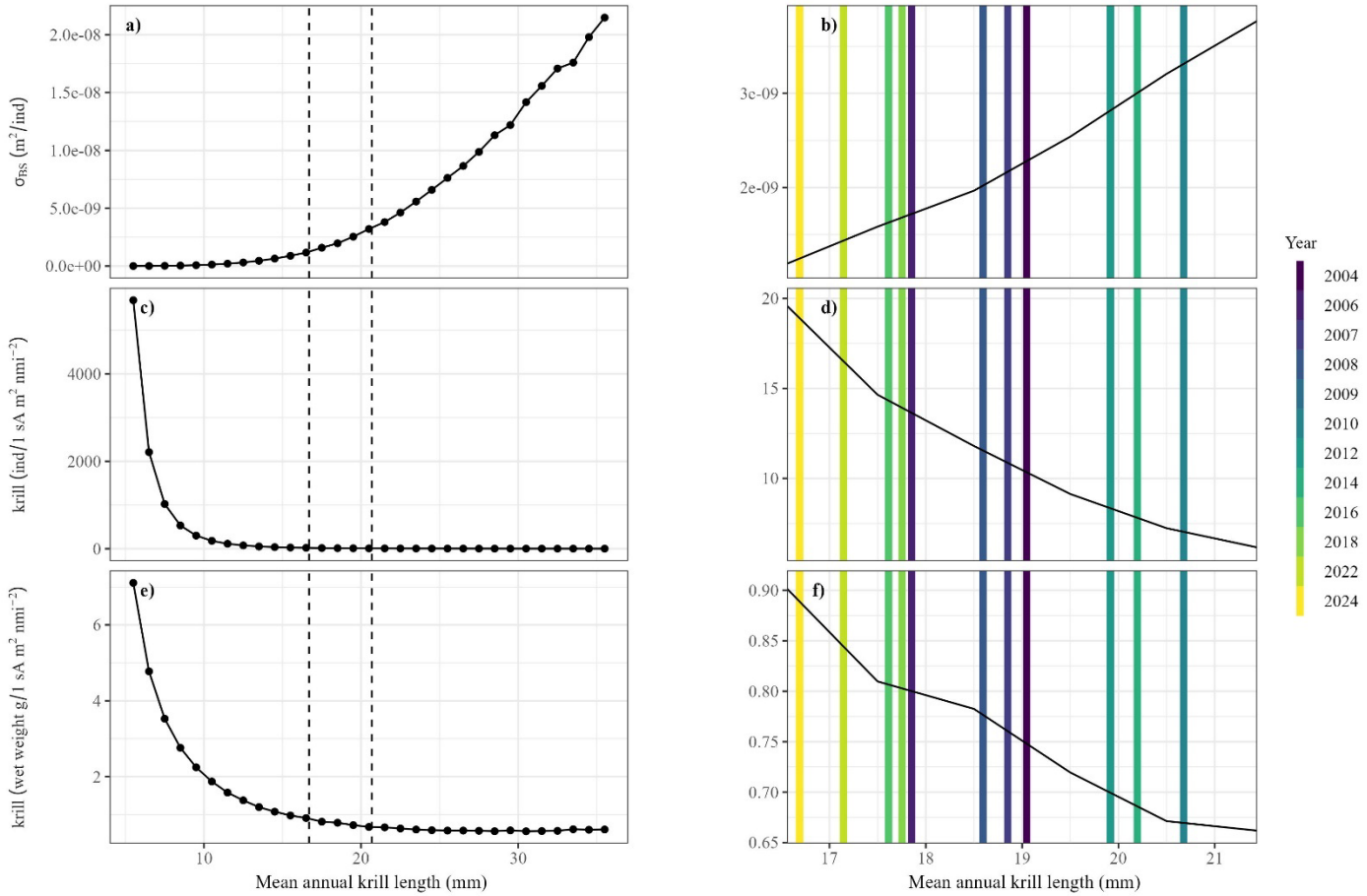


Figure A1.12. Effect of the mean annual krill length estimate on a) and b) σ_{bs}, c) and d) krill density, and e) and f) krill wet weight. Mean observed annual krill lengths are indicated by colored vertical bars (n = 12 years) in panels b), d) and f). Note that panels b), d), and f) are expanded views of the krill lengths within the vertical dashed lines in panels a), c), and e).

Appendix II: modeling krill TS

Introduction

Converting krill acoustic backscatter measurements to density requires knowledge of how individual krill scatter sound. For quantitative acoustic surveys of krill density, physics-based scattering models are the most common way to estimate TS (e.g., Conti and Demer 2006, Reiss et al. 2008, Ressler et al. 2012), as opposed to acoustic surveys of fish, where observations of *in situ* TS or empirical length-TS relationships are more common (Simmonds and MacLennan, 2005). TS models have historically been a major source of uncertainty in krill density estimation (Stanton and Chu 2000), including in the historical method used in the EBS time series (Ressler et al. 2012, Smith et al. 2013). Here, we describe the parameterization of an updated EBS krill TS model (Lucca et al. 2021; 2023) using additional measurements of material properties, *in situ* tilt, and body shape for regionally observed species (*T. inermis*, *T. spinifera*, and *T. raschii*), along with a resampling procedure. While this Appendix describes the parameterization for both EBS and GOA krill TS, only the EBS krill results are used in this document in the "updated method"; the GOA TS results will be applied to GOA survey data at a later date. We also demonstrate how to implement model parameterization using the *acousticTS* R package (Lucca 2023).

SDWBA model

Krill TS was calculated using the stochastic distorted-wave Born approximation (SDWBA), which accounts for distortions of the incident and scattered sound waves due to body shape complexity (Demer and Conti, 2003; Conti and Demer, 2006). This approach requires

discretizing animal body shapes (r_0) into deformed cylinders. The linear scattering coefficient, $F_{\mathrm{bs}_j}(\theta, f)$, for the j^{th} cylinder is expressed as:

$$\mathcal{F}_{bs_j}(\theta, f) = \frac{k_1(f)}{4} \int_{r_0} \left(\gamma_k - \gamma_\rho\right) e^{-2i\vec{k}_i(f)\vec{r}_0} \frac{a_j J_1(2k_2(f) a_j \cos\beta_{tilt})}{\cos\beta_{tilt}} dr_0, \quad (Eq. 2.1)$$

where f is the transmit frequency (Hz), θ is the orientation relative to the incident soundwave (with broadside incidence at $\frac{\pi}{2}$ radians), $i = \sqrt{-1}$, k is the acoustic wavenumber (with subscripts "1" and "2" representing the surrounding medium and animal body, respectively), J_1 is the cylindrical Bessel function of the first kind of order 1, a is the radius (m), $\vec{r}_0$ is the rotated body shape matrix, and β_{tilt} is the tilt angle of each cylinder relative to the central axis of $\vec{r}_0$.

The material properties are incorporated via the $\left(\gamma_\kappa\text{-}\gamma_\rho\right)$ term where:

$$\gamma_\kappa - \gamma_\rho = \frac{1}{gh^2} + \frac{1}{g^2} - 2. \quad (\text{Eq. 2.2})$$

which is equivalent to the M parameter expressed in Smith et al. (2013) and Lucca et al. (2021). Here g and h denote the density and sound speed contrasts, respectively. Lastly, $\vec{k}_i$ is the rotated incident wave number vector:

$$\vec{k}_i(f) = k_1(f) \begin{bmatrix} \sin\theta \\ 0 \\ \cos\theta \end{bmatrix}. \quad (\text{Eq 2.3})$$

The integrated linear backscatter, $\mathcal{F}_{\mathrm{bs}}(\theta, \mathrm{f})$, can be calculated via:

$$\mathcal{F}_{bs}(\theta, f) = \sum_{j=1}^{N_{cyl}} \mathcal{F}_{bs_j}(\theta, f) e^{i\varphi_j}. \quad (\text{Eq. 2.4})$$

where N_{cyl} is the number of cylinders. Here, the phase deviation φ_j is applied to each cylinder. This can then be used to derive TS:

$$TS(\theta, f) = 10log_{10}|\mathcal{F}_{bs}(\theta, f)|^2. \quad \text{(Eq. 2.5)}$$

SDWBA model parameterization

Body shape

Average body shapes for the Eastern Bering Sea (EBS, *n* = 224) and Gulf of Alaska (GOA, *n* = 317) computed from mixed samples of *Thysanoessa inermis* (*n* = 74), *T. raschii* (*n* = 109), *T. spinifera* (*n* = 234), and *Euphausia pacifica* (*n* = 124) (Lucca et al., 2021, their Figures 2 and 4; 2023) are represented in Table A2.1. These shapes are normalized based on animal standard length 2 ($SL2$, mm; Mauchline, 1980) where the along-body coordinates, x, are bounded by $[0,1]$. These shapes are further normalized to the body center-line such that:

$$r_0 = \begin{bmatrix} x_1 & x_2 & \dots & x_{N_{cyl}} \\ 0 & 0 & \dots & 0 \\ 0 & 0 & \dots & 0 \end{bmatrix}. \quad (Eq. 2.6)$$

Scattering parameters

Values for g and h were drawn from Normal distributions $\left(\mathcal{N}(\mu, \sigma^2)\right)$ specific to EBS and GOA specimens (Table A2.2; Lucca et al., 2021), where μ is the mean and σ the S.D. Daytime stereo camera measurements from Lucca et al. (2021) were used for drawing θ from a von Mises $\left(vM(\mu, \kappa)\right)$, where μ and κ are the location (or mean direction) and shape (or concentration) parameters, respectively. The ratio between the body radius-of-curvature and length, ρ_c, was

simulated using a truncated Normal $\left(\mathcal{TN}_{[a,b]}(\mu, \sigma^2)\right)$ computed from the flexure of tethered specimens in Lucca et al. (2023), where *a* and *b* correspond to the lower and upper bounds of the truncated distribution. The mean and S.D. were calculated using all krill represented in Table 3 from Lucca et al. (2023). The distribution was bounded by $[2,10]$, which was estimated using the approximate range of mean ± 1 S.D. estimates of all krill from the same table. This range further corresponds to a realistic range in ρ_c estimates reported elsewhere in the krill TS modeling literature (e.g., Lawson et al., 2006). It is also worth noting that the krill body shape quickly flattens as ρ_c increases, so $\rho_c = 10$ effectively translates to a krill with a very slight curvature. The TS offset, $G_{\Delta TS}$, represents the *t*-distribution of observed differences in krill TS when comparing modeled predictions and empirical measurements at 120 kHz (Lucca et al., 2023), the frequency currently used for echo integration and estimation of density. This quantity is added to the modeled TS predictions in the logarithmic domain.

Shape curvature transformation

Simulated ρ_c is applied to uniformly "bend" r_0 according to the circular-arc geometry of an osculating circle (Stanton, 1989). Values are calculated along the curvilinear axis via:

$$\xi_i = -\phi + 2\frac{i-1}{N_{cyl}-1}, i = 1,2,\ldots,N_{cyl}, \quad (Eq.\,2.7)$$

where $\xi_i \in [-\phi, \phi]$ and ϕ is the maximum curvature angle: $\frac{1}{2\rho_c}$. The arc position for the x- and z-axes can then be expressed by $\hat{x_i}$ and $\hat{z_i}$, respectively:

$$\hat{x}_i = (\rho_c \times L)\ sin\,\xi_i + \frac{L}{2} \quad (Eq.\,2.8)$$

$$\hat{z}_i = (\rho_c \times L)\ 1 - cos\,\xi_i \quad (Eq.\,2.9)$$

The curved position matrix becomes:

$$\hat{r}_0 = \begin{bmatrix} \hat{x}_1 & \hat{x}_2 & \dots & \hat{x}_{N_{cyl}} \\ 0 & 0 & \dots & 0 \\ \hat{z}_1 & \hat{z}_2 & \dots & \hat{z}_{N_{cyl}} \end{bmatrix}. \quad (Eq. 2.10)$$

Stochastic phase variability

The SDWBA adjusts the number of cylinders comprising r_0 to maintain constant ratio between the body shape spatial resolution and wavelength, λ (Conti and Demer, 2006). This requires defining a reference body length (L_0, mm), cylinder count (N_0), and frequency (f_0, Hz). The resampled number of cylinders within r_0 $\hat{N}_{\text{cyl}}(f, L)$ is defined by:

$$\hat{N}_{cyl}(f, L) = N_0 \frac{fL}{f_0 L_0}. \quad (Eq. 2.11)$$

Therefore, $\widehat{r_0}$ yields the resampled position matrix,$\widehat{r_0^{\star}}$:

$$\widehat{r_0} \in R^{N_{cyl} \times 3} \rightarrow \widehat{r_0^{\star}} \in R^{\hat{N}_{\text{cyl}}(f,L) \times 3}, \quad \text{(Eq. 2.12)}$$

where each row represents the (x, y, z) coordinates of a cylindrical segment.

The reference phase deviation, $\sigma_{\varphi 0}$ (radians), is computed from the SNR:

$$\sigma_{\varphi_0} = \frac{1}{\sqrt{2 \times 10^{SNR_{dB}/10}}}. \quad \text{(Eq. 2.13)}$$

For instance, the SNR for backscatter measurements at 120 kHz from Lucca et al. (2023) was ~ 7.2 dB, which corresponded to $\sigma_{\varphi 0} \approx 0.31$ radians at 120 kHz. Similar to $\hat{N}_{\text{cyl}}(f, L)$, this is recalculated via:

$$\sigma_{\varphi} = \sigma_{\varphi_0} \frac{N_0 L}{\widehat{N}_{cyl}(f, L) L_0}, \qquad Eq.\ 2.14)$$

which is then used to draw φ_j from a Standard Normal $\left(N(0, \varphi_0)\right)$.

Modeled TS estimates from the SDWBA are averaged over multiple iterations to effectively "smooth" phase variability. For instance, this can be visualized by simulating $TS(f)$ for a 25 mm krill with a high degree of curvature (ρ_c = 0.33), a length-to-radius ratio of 12.2 at broadside incidence $\theta = \frac{\pi}{2}$, and fluid-like material properties (g = 1.018, h = 1.021) (Figure A2.1). This illustrates how sensitive $TS(f)$ estimates are to the defined number of iterations ($n_{\text{iterations}}$). For this krill, $TS(f)$ estimates become relatively "stable" at $n_{\text{iterations}} \geq 100$.

Spectral averaging

A bandpass filter was applied to predicted TS based on the transmitted pulse duration (τ, seconds) with bandwidth B ($B \sim \frac{1}{\tau}$, Hz) around a center frequency (f_c, Hz). This bandwidth was discretized over N_f frequencies (f_i) (for the current study, $\tau = 512^{-6}$ seconds, $f_c = 120^3$ Hz, and N_f = 10). The spectrally-averaged TS, $\langle TS(\theta) \rangle$, is defined by:

$$\langle TS(\theta, f_c) \rangle \ = \ G_{\Delta TS} + \frac{1}{N_f} \sum_{i\,=\,1}^{n_f} TS(\theta, f_i), \quad (Eq.\ 2.15)$$

where the discrete frequencies (Hz) are:

$$f_i \ = \ f_c \ - \ \frac{B}{2} \ + \ (i - 1) \frac{B}{N_f - 1}, \quad (Eq.\ 2.16)$$

for i = 1,2, … , N_f.

Implementation using *acousticTS* in *R*

This section describes how to implement the above model parameterization using the acousticTS R-package (Lucca 2023). Note that the below simulation is similar to that implemented in the updated method, but the parameters determining the total number of simulations (n_iterations and n_realizations, below) are set much lower for demonstration purposes in the below example (n_iterations is set at 100 in the example vs 1,000 in our actual parameterization, and n_realizations is set at 1,000 in the example vs 10,000 in our parameterization).

Preparing for simulations

First we load in a few packages that will be needed for later processing.

```
# Libraries used in processing
# ----------------------------
library(acousticTS)
library(circular)
library(tidyverse)
library(truncnorm)
```

We can then read in the two pre-generated `.RData` objects. These comprise `FLS`-class expressions for EBS and GOA krill, which are both a type of subclass belonging to the parent `scatterer`-class (to see the help for this function type `?scatterer-class`).

```
# Load RData objects with pre-loaded `FLS` objects
# ------------------------------------------------
load("/data/GOA_krill.RData")
load("/data/EBS_krill.RData")
```

Basic information about these objects can be accessed using generic methods like `show` and `plot`. For instance, typing `EBS_krill` into the R terminal yields:

```
> EBS_krill
FLS-object
  Fluid-like scatterer
   ID: UID
 Body dimensions:
  Length: 1 m (n = 17 cylinders)
  Mean radius: 0.0552 m
  Max radius: 0.082 m
 Shape parameters:
  Defined shape: arbitrary
  L/a ratio: 12.2
  Taper order:
 Material properties:
  g: 1.018
  h: 1.021
 Body orientation (relative to transducer face/axis): 1.571 radians
```

As indicated in Table A2.1, these shapes are normalized to the maximum body length and can be readily modified for simulations. They are further centered to remove along-body curvature for standardization. Similarly, ***plot(EBS_krill)*** produces a visualization of the along-axis segments comprising the overall krill body shape (Figure A2.2).

```
> plot(EBS_krill)
```

Simulating TS

Once the EBS and GOA *FLS*-class objects are loaded, we can begin to parameterize the simulation workflow. This includes general acoustic parameters and other variables required for the SDWBA, as well as other arguments for the ***simulate_ts*** function (see: ***?simulate_ts***).

```
# Define processing parameters
# ------------------------------------------------------------------
-------
# General processing parameters required for the TS simulation
# ------------------------------------------------------------------
-------
# General
# -------
```

```r
# Transmit frequency (center) [Hz]
frequency <- 120e3
# Transmit pulse duration [s]
τ <- 512e-6
# Bandpass filter resolution [Dimensionless]
N_bandpass <- 10
# Seawater sound speed [m s^-1]
sound_speed_sw <- 1470
# Seawater density [kg m^-3]
density_sw <- 1025
# ------------------------
# SDWBA-specific parameters
# ------------------------
# Number of realizations ran to compute each TS value [Dimensionless]
n_iterations <- 100
# Reference along-body cylinder count [Dimensionless]
n_segments_init <- 15
# Reference length [m]
length_init <- 17.9e-3
# Reference frequency [Hz]
frequency_init <- 120e3
# Reference phase deviation [radians]
σφ_init <- 0.31
# -----------------
# Function arguments
# -----------------
# Number of simulated TS values [Dimensionless]
n_realizations <- 1000
# Batch variable used to define the groupby functionality
# ---- This dictates that `n_realizations` is done for each value of
# ---- the argument `batch_params`
batch_by <- "length"
# Define the appropriate model
model <- "SDWBA_curved"
# Toggle function verbosity
verbose <- TRUE
# Toggle parallelization
# ---- NOTE: if toggled, this requires an appropriate installation of
the
# ---- `pbapply` package. There may be some issues with
parallelization
# ---- for specific OS and OS versions
parallel <- TRUE
```

We then have to define our parameter distributions (Table A2.2). Some of these are shared across our datasets, so we can define these here. These are stored within a *list* that is passed to the *parameters* argument in the *simulate_ts* function. We can provide vectors of values (e.g., L) or generating functions that draw a sample from pre-defined probability distribution functions (e.g., θ, ρ_c, $G_{\Delta TS}$).

```
# Simulate distributions
# ------------------------------------------------------------------
-------
# The defined distributions can either be in the form of generative
functions
# or pre-defined vectors/distributions
# ------------------------------------------------------------------
-------
# Global
# ------
# Lengths [mm]
# ---- This is a sequence of length values. These are automatically
expanded
# ---- across the number of iterations defined in the associated
simulation
# ---- function
#   start with a sequence of Poland lengths (5.5 - 35.5 mm)

length_type_conversions <- data.frame('poland_mm' = seq(5.5, 35.5, 1))

# convert to SL1 lengths

length_type_conversions$SL1_mm <- 1.07 *
length_type_conversions$poland_mm + 0.1041

# convert to SL2 lengths

length_type_conversions$SL2_mm <- 0.82 *
length_type_conversions$SL1_mm + -0.2

# use SL2 lengths as the model lengths

lengths <- length_type_conversions$SL2_mm * 1e-3


# Orientation: von Mises (or Circular Normal) [radians]
```

```
θ <- function() rvonmises(n=1, mu=circular(1.66), kappa=2.80,
                          control.circular=list(units="radians"))
# Radius-of-curvature ratio (relative to body length) [Dimensionless]
ρc <- function() rtruncnorm(n=1, a=2.00, b=10.00, mean=6.10, sd=2.9)
# Empirical TS gain/offset [dB]
G_mean <- 2.5 # Mean
G_sigma <- 0.3 # Standard deviation
G_df <- 111 # Degrees of freedom from empirical measurements
GΔTS <- function() G_mean + G_sigma * rt(1, df=G_df)
```

There are also parameters like g and h that are specific to EBS and GOA krill, so we can incorporate these into the aforementioned ***list*** objects.

```
# Simulate distributions [region]
# -------------------------------
# EBS
# ---
EBS_params = list(
    length=lengths,
    sound_speed_sw = sound_speed_sw,
    density_sw = density_sw,
    g = function() rnorm(1, 1.018, 0.006),
    h = function() rnorm(1, 1.022, 0.006),
    theta = θ,
    radius_curvature_ratio = ρc,
    phase_sd_init = σφ_init,
    n_iterations = n_iterations,
    n_segments_init = n_segments_init,
    length_init = length_init,
    frequency_init = frequency_init
)
# ---
# GOA
# ---
GOA_params = list(
    length=lengths,
    sound_speed_sw = sound_speed_sw,
    density_sw = density_sw,
    g = function() rnorm(1, 1.021, 0.006),
    h = function() rnorm(1, 1.037, 0.018),
    theta = θ,
    radius_curvature_ratio = ρc,
    phase_sd_init = σφ_init,
    n_iterations = n_iterations,
```

```
    n_segments_init = n_segments_init,
    length_init = length_init,
    frequency_init = frequency_init
)
```

The last required variable we need to prepare is the defined frequency range, which needs to incorporate the bandpass filter. This simply requires providing ***simulate_ts*** with the appropriate bandwidth to compute TS over rather than just the center frequency (i.e. 120 kHz).

```
# Bandwidth [Hz]
B <- 1 / τ
frequency_range <- seq(frequency - B/2,
                       frequency + B/2,
                       length.out=N_bandpass)
```

With all of the parameters and variables initialized and assigned, we can begin simulating TS.

```
# Simulate TS values
# ------------------------------------------------------------------
-------
# This will generate a `data.frame` object with the defined parameters
and
# resulting TS values
# ------------------------------------------------------------------
-------
# EBS
# ---
EBS_ts_df <- simulate_ts(
    object = EBS_krill,
    batch_by = batch_by,
    n_realizations = n_realizations,
    frequency = frequency_range,
    model = model,
    parameters = EBS_params,
    parallel = parallel,
    verbose = verbose
)
# ---
# GOA
# ---
GOA_ts_df <- simulate_ts(
    object = GOA_krill,
```

```
    batch_by = batch_by,
    n_realizations = n_realizations,
    frequency = frequency_range,
    model = model,
    parameters = GOA_params,
    parallel = parallel,
    verbose = verbose
)
```

When *verbose=TRUE*, occasional updates will be supplied to the terminal (including a progressbar), e.g.

```
> EBS_ts_df <- simulate_ts(
+   object = EBS_krill,
+   batch_by = batch_by,
+   n_realizations = n_realizations,
+   frequency = frequency_range,
+   model = model,
+   parameters = EBS_params,
+   parallel = parallel,
+   verbose = verbose
+ )
===================================
Scatterer-class: FLS
Model(s): SDWBA_curved
Batching parameter(s): length
Simulated parameters: length, sound_speed_sw, density_sw, g, h, theta,
radius_curvature_ratio, phase_sd_init, n_iterations, n_segments_init,
length_init, frequency_init
Total simulation realizations: 31000
Parallelize TS calculations: TRUE
===================================
===================================
Preparing parallelized simulations
Number of cores: 11
socket cluster with 11 nodes on host 'localhost'
  |++++++++++++++++++++++++++++++++++++++++++++++++++| 100%
===================================
Simulations complete!
===================================
```

The ***simulate_ts*** function ingests the parameters within the ***EBS_params*** and ***GOA_params*** to modify ***EBS_krill*** and ***GOA_krill***, respectively, to calculate TS. The output is a ***list[data.frame]***.

```
> tibble(EBS_ts_df$SDWBA_curved) %>% print(n=5)
# A tibble: 310,000 × 20
  model    realization length_idx length sound_speed_sw density_sw
g     h theta radius_curvature_ratio phase_sd_init n_iterations
n_segments_init
  <chr>          <int>      <int>  <dbl>          <dbl>      <dbl>
<dbl> <dbl> <dbl>                  <dbl>          <dbl>       <dbl>
<dbl>
1 SDWBA_c…           1          1  0.005           1500       1026
1.02  1.03  2.36                   9.16          0.31         100
15
2 SDWBA_c…           1          1  0.005           1500       1026
1.02  1.03  2.36                   9.16          0.31         100
15
3 SDWBA_c…           1          1  0.005           1500       1026
1.02  1.03  2.36                   9.16          0.31         100
15
4 SDWBA_c…           1          1  0.005           1500       1026
1.02  1.03  2.36                   9.16          0.31         100
15
5 SDWBA_c…           1          1  0.005           1500       1026
1.02  1.03  2.36                   9.16          0.31         100
15
# ℹ 309,995 more rows
# ℹ 7 more variables: length_init <dbl>, frequency_init <dbl>,
frequency <dbl>, f_bs <cpl>, sigma_bs <dbl>, TS <dbl>, TS_sd <dbl>
# ℹ Use `print(n = ...)` to see more rows
```

Evaluating the TS-length relationship

With the predicted TS values successfully simulated, we can then aggregate the values to compute the spectral averaged TS for each realization so we can apply $G_{\Delta TS}$.

```
# Light processing
# ----------------
# EBS
```

```r
# ---
EBS_ts_df$SDWBA_curved %>%
  as_tibble() %>%
  group_by(realization, length) %>%
  reframe(TS = 10*log10(mean(sigma_bs))) %>%
  rowwise() %>%
  mutate(G=GΔTS()) %>%
  ungroup() %>%
  mutate(TS_final=TS + G) -> EBS_ts_proc
# ---
# GOA
# ---
GOA_ts_df$SDWBA_curved %>%
  as_tibble() %>%
  group_by(realization, length) %>%
  reframe(TS = 10*log10(mean(sigma_bs))) %>%
  rowwise() %>%
  mutate(G=GΔTS()) %>%
  ungroup() %>%
  mutate(TS_final=TS + G) -> GOA_ts_proc
```

Some initial plotting can generate some insights into the general trends, as well as the very large degrees of uncertainty in the predictions (Figure A2.3).

```r
# Initial plotting
# ----------------
bind_rows(EBS_ts_proc %>% mutate(Region = "EBS"),
          GOA_ts_proc %>% mutate(Region = "GOA")) %>%
  ggplot() +
  geom_violin(
    mapping = aes(x=length * 1e3, y=TS_final, group=length)
  ) +
  facet_wrap(~Region, nrow=2) +
  theme_minimal() +
  labs(x = "Length (mm)",
       y = expression(TS~(dB~re~1~m^2))) -> base_layer
base_layer
```

Appendix II Tables and Figures

Table A2.1. Generic krill shapes for Gulf of Alaska (GOA) and Eastern Bering Sea (EBS).

	x		y	z	a	
	GOA	**EBS**			**GOA**	**EBS**
1	0.00000	0.00000	0	0	0.02579	0.02862
2	0.05997	0.05648	0	0	0.05163	0.05706
3	0.12293	0.12007	0	0	0.06551	0.06988
4	0.18567	0.18318	0	0	0.07282	0.07797
5	0.24779	0.24680	0	0	0.07538	0.08202
6	0.31131	0.31005	0	0	0.06884	0.07981
7	0.37363	0.37335	0	0	0.06049	0.07150
8	0.43609	0.43692	0	0	0.05638	0.06362
9	0.49894	0.50032	0	0	0.05457	0.06222
10	0.56151	0.56379	0	0	0.05110	0.06045
11	0.62360	0.62724	0	0	0.04747	0.05859
12	0.68645	0.69033	0	0	0.04409	0.05510
13	0.74894	0.75388	0	0	0.03893	0.05095
14	0.81191	0.81752	0	0	0.03326	0.04625
15	0.87490	0.88033	0	0	0.02761	0.04085
16	0.93985	0.94399	0	0	0.02422	0.03338
17	1.00000	1.00000	0	0	0.00000	0.00000

Note: The left-most numeric column represents individual points that inform the discrete cylindrical segments along the animal's body. The x, y, and z coordinates are normalized to the body length, with y and z coordinates normalized to the animal's centerline. Radii (a) are provided for both Gulf of Alaska (GOA) and Eastern Bering Sea (EBS) populations.

Table A2.2. Model parameter distributions and value used for predicting krill TS. Material properties (g and h) were drawn from distributions specific to each region. Values for orientation (θ), radius-of-curvature ratio (ρ_c) and TS offset at 120 kHz ($G_{\Delta TS}$) were drawn from global distributions. The SDWBA parameters correspond to the relative frequency (f_0), number of cylinders (N_0), length (L_0), and phase deviation (σ_φ).

Parameters	Units	EBS	GOA
g	Dimensionless	$\mathcal{N}(1.018, 0.006^2)$	$\mathcal{N}(1.021, 0.006^2)$
h	Dimensionless	$\mathcal{N}(1.022, 0.018^2)$	$\mathcal{N}(1.037, 0.011^2)$
θ	Radians	$v\mathcal{M}(1.66, 2.8)$	
ρ_c	Dimensionless	$\mathcal{TN}_{[2,10]}(6.1, 2.9^2)$	
$G_{\Delta TS}$	dB	$t_{111}(2.5, 0.3)$	
SDWBA parameters			
f_0	Hz	$120,000$	
N_0	Dimensionless	15	
L_0	mm	17.9	
σ_{φ_0}	Radians	0.31	
φ_j	Radians	$\mathcal{N}(0, \sigma_\varphi)$	
Bandpass filter parameters			
τ	ms	500	
f_c	Hz	$120,000$	
N_f	Dimensionless	20	

Note: statistical distributions are expressed the following notation: $\mathcal{N}$: Normal; $v\mathcal{M}$: von Mises; $\mathcal{TN}$: Truncated Normal; t: non-standardized Student's t.

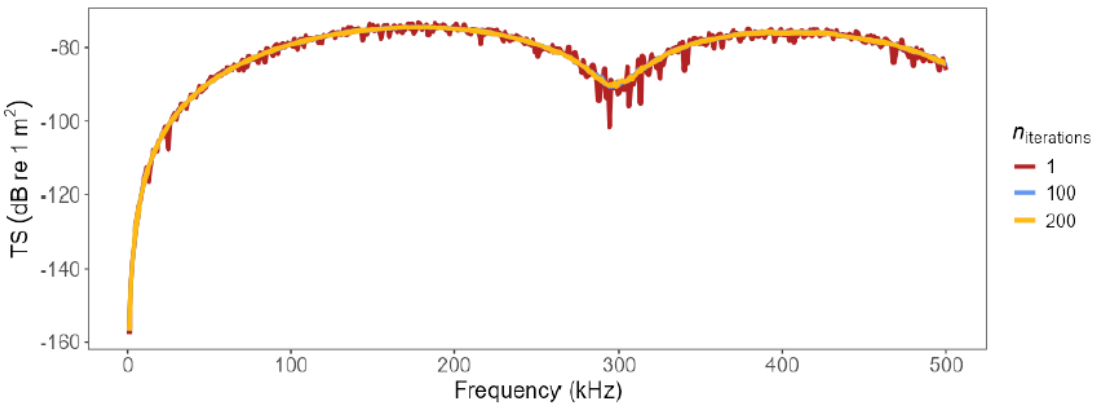


Figure A2.1. Example TS-frequency spectrum (1 - 500 kHz at a 1 kHz resolution) showing how mean TS(f) varies with an increasing number of iterations ($n_{iterations}$).

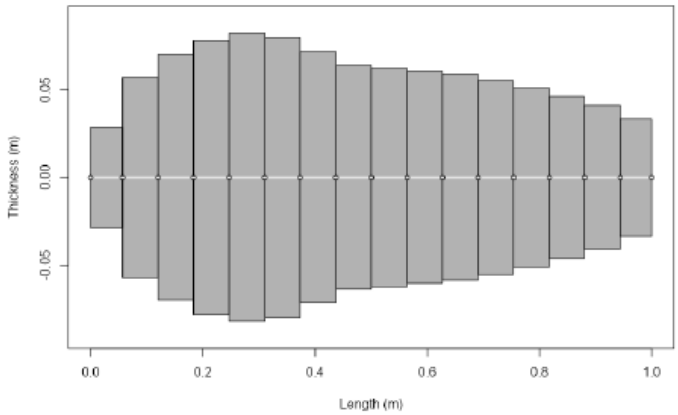


Figure A2.2. Example 'FLS'-class object representing a normalized EBS krill shape. Each gray polygon corresponds to an approximation of each cylinder used to discretize the body's position matrix.

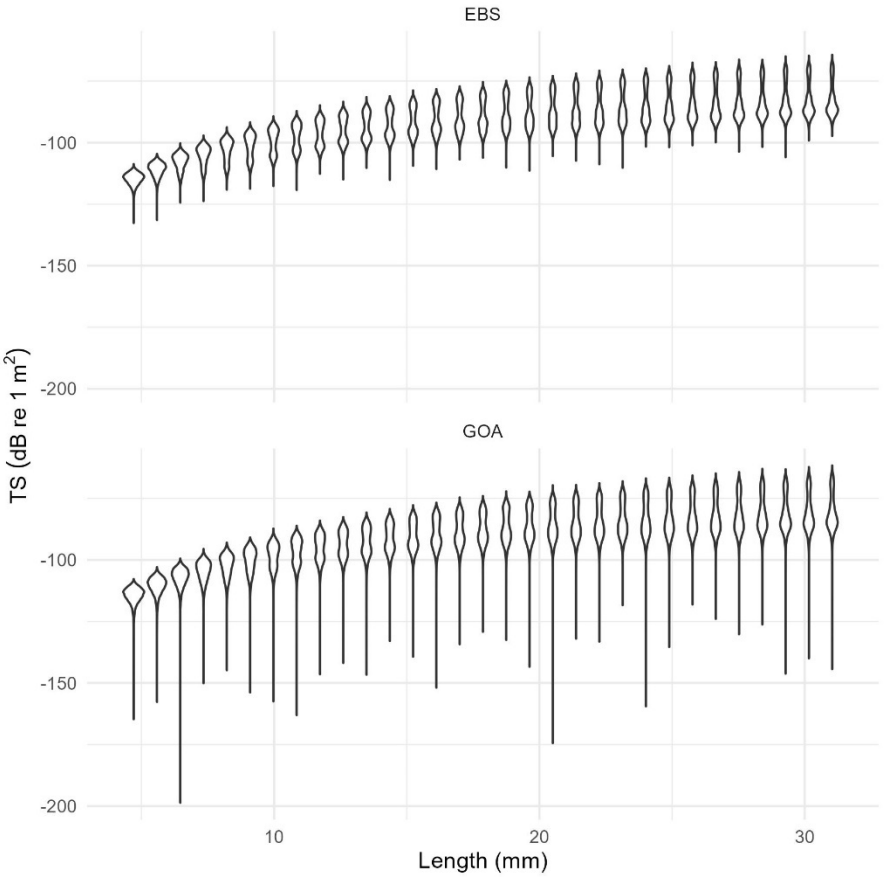


Figure A2.3. Violin plots visualizing the spread of TS for each length *L* when simulated for EBS (top) and GOA (bottom) krill.

Acknowledgments

Thoughtful reviews and comments from Jon Reum, Robert Levine, and Sandy Parker-Stetter greatly improved this manuscript.

References

Amakasu, K., Mukai, T., and Moteki, M. 2017. Measurement of the volume-backscattering spectrum from an aggregation of Antarctic krill and inference of their length-frequency distribution. Polar Science 12:79-87.

Aydin, K., and F. Mueter. 2007. The Bering Sea-A dynamic food web perspective. Deep-Sea Research Part II: Topical Studies in Oceanography 54:2501–2525.

Bassett, C., De Robertis, A., and Gallagher, M. 2024. A passive acoustic drifter for radiated noise measurements of NOAA Fisheries survey vessels. U.S. Department of Commerce, NOAA Technical Memorandum NMFS-AFSC-490.

Brodeur, R. D., M. T. Wilson, L. Ciannelli, M. Doyle, and J. M. Napp. 2002. Interannual and regional variability in distribution and ecology of juvenile pollock and their prey in frontal structures of the Bering Sea. Deep-Sea Research II 49:6051–6067.

Cochrane, N. A., D. Sameoto, A. W. Herman, and J. Neilson. 1991. Multiple-Frequency Acoustic Backscattering and Zooplankton Aggregations in the Inner Scotian Shelf Basins. Canadian Journal of Fisheries and Aquatic Sciences 48:340–355.

Conti, S. G., and Demer, D. A. 2006. Improved parameterization of the SDWBA for estimating krill target strength. ICES Journal of Marine Science, 63:928-935.

Coyle, K. O. 2000. Acoustic estimates of zooplankton biomass and distribution: application of canonical correlation to scaling of multifrequency acoustic data. Canadian Journal of Fisheries and Aquatic Sciences 57:2306-2318.

Coyle, K. O., and A. I. Pinchuk. 2002. The abundance and distribution of euphausiids and zero-age pollock on the inner shelf of the southeast Bering Sea near the Inner Front in 1997–1999. Deep Sea Research II 49:6009–6030.

Demer, D. A., and S. G. Conti. 2003. Validation of the stochastic distorted-wave Born approximation model with broad bandwidth total target strength measurements of Antarctic krill. ICES Journal of Marine Science 60:625–635.

De Robertis, A., and I. Higginbottom. 2007. A post-processing technique to estimate the signal-to-noise ratio and remove echosounder background noise. ICES Journal of Marine Science 64:1281–1291.

De Robertis, A., D. R. McKelvey, and P. H. Ressler. 2010. Development and application of an empirical multifrequency method for backscatter classification. Canadian Journal of Fisheries and Aquatic Sciences 67:1459–1474.

Decker, M., and G. Hunt. 1996. Foraging by murres (*Uria* spp.) at tidal fronts surrounding the Pribilof Islands, Alaska, USA. Marine Ecology Progress Series 139:1–10.

Harvey, H. R., R. L. Pleuthner, E. J. Lessard, M. J. Bernhardt, and C. Tracy Shaw. 2012. Physical and biochemical properties of the euphausiids *Thysanoessa inermis*, *Thysanoessa raschii*, and *Thysanoessa longipes* in the Eastern Bering Sea. Deep Sea Research Part II: Topical Studies in Oceanography 65–70:173–183.

Holliday, D. V., and R. E. Pieper. 1995. Bioacoustical oceanography at high frequencies. ICES Journal of Marine Science 52:279–296.

Hunt, G. L., C. Baduini, and J. Jahncke. 2002. Diets of short-tailed shearwaters in the southeastern Bering Sea. Deep Sea Research Part II: Topical Studies in Oceanography 49:6147–6156.

Hunt, G. L., P. H. Ressler, G. A. Gibson, A. De Robertis, K. Aydin, M. F. Sigler, I. Ortiz, E. J. Lessard, B. C. Williams, A. Pinchuk, and T. Buckley. 2016. Euphausiids in the Eastern Bering Sea: A synthesis of recent studies of euphausiid production, consumption and population control. Deep Sea Research Part II: Topical Studies in Oceanography 134:204–222.

Ianelli, J., T. Honkalehto, S. Wassermann, A. McCarthy, S. Steinessen, C. McGilliard, and E. Siddon. 2024. Assessment of walleye pollock in the Eastern Bering Sea.

Jarvis, T., N. Kelly, S. Kawaguchi, E. van Wijk, and S. Nicol. 2010. Acoustic characterisation of the broad-scale distribution and abundance of Antarctic krill (*Euphausia superba*) off East Antarctica (30-80°E) in January-March 2006. Deep Sea Research Part II: Topical Studies in Oceanography 57:916–933.

Korneliussen, R. 2000. Measurement and removal of echo integration noise. ICES Journal of Marine Science 57:1204–1217.

Lang, G. M., P. A. Livingston, and K. A. Dodd. 2005. Groundfish food habits and predation on commercially important prey species in the Eastern Bering Sea from 1997 through 2001. United States Department of Commerce, NOAA Technical Memorandum NMFS-AFSC-158:249.

Lavery, A. C., P. H. Wiebe, T. K. Stanton, G. L. Lawson, M. C. Benfield, and N. Copley. 2007. Determining dominant scatterers of sound in mixed zooplankton populations. The Journal of the Acoustical Society of America 122:3304–3326.

Lawson, G.L., Wiebe, P.H., Ashjian, C.J., Chu, D., and Stanton, T.K. 2006. Improved parameterization of Antarctic krill target strength models. The Journal of the Acoustical Society of America 119:232-242.

Lawson, G. L., P. H. Wiebe, T. K. Stanton, and C. J. Ashjian. 2008. Euphausiid distribution along the Western Antarctic Peninsula-Part A: Development of robust multi-frequency acoustic techniques to identify euphausiid aggregations and quantify euphausiid size, abundance, and biomass. Deep Sea Research Part II: Topical Studies in Oceanography 55:412–431.

Levine, M., and A. De Robertis. 2025. Making do with less: Extending an acoustic-based time series of euphausiid abundance using an uncrewed surface vehicle with fewer frequencies. Fisheries Research 282:107270.

Levine, M., and P. Ressler. 2024. Eastern Bering Sea Euphausiids (‘Krill’). In: Siddon, E. 2024. Ecosystem Status Report 2024: Eastern Bering Sea, Stock Assessment and Fishery Evaluation Report, North Pacific Fishery Management Council, 1007 West 3rd Ave., Suite 400, Anchorage, Alaska 99501.

Levine, M., Williams, K., and P. Ressler. 2018. Measuring the in situ tilt orientation of fish and zooplankton using stereo photogrammetric methods. Limnology and Oceanography: Methods 16:390-399.

Levine, R., De Robertis, A., Grunbaum, D., Wildes, S., Farley, E., Stabeno, P. J., and Wilson, C. D. 2023. Climate-driven shifts in the pelagic fish community of the Chukchi Sea. Deep-Sea Research II 208:105244

Lucca, B. M., P. H. Ressler, H. R. Harvey, and J. D. Warren. 2021. Individual variability in sub-Arctic krill material properties, lipid composition, and other scattering model inputs affect acoustic estimates of their population. ICES Journal of Marine Science 78:1470–1484.

Lucca, B. M., P. H. Ressler, and J. D. Warren. 2023. Target strength measurements of individual sub-Arctic krill have frequency-dependent differences from scattering model predictions. The Journal of the Acoustical Society of America 154:3374-3387.

Lucca, B. 2023. acousticTS: An R package for calculating the theoretical acoustic target strength of individual targets. (v.1.0). Zenodo. https://doi.org/10.5281/zenodo.7600660

MacLennan, D. N., P. G. Fernandes, and J. Dalen. 2002. A consistent approach to definitions and symbols in fisheries acoustics. ICES Journal of Marine Science 59:365–369.

Madureira, L. S. P., I. Everson, and E. J. Murphy. 1993. Interpretation of acoustic data at two frequencies to discriminate between Antarctic krill (*Euphausia superba* Dana) and other scatterers. Journal of Plankton Research 15:787–802.

Mauchline, J. 1980. The biology of mysids and euphausiids. Advances in Marine Biology 18:1–681.

McGowan, D. W., D. T. Jones, and M. Levine. 2025. Results of the acoustic-trawl survey of walleye pollock (*Gadus chalcogrammus*) in the Gulf of Alaska, (DY2023-08). AFSC Processed Rep. 2025-08, 111 p. Alaska Fish. Sci. Cent., NOAA, Natl. Mar. Fish. Serv., 7600 Sand Point Way NE, Seattle WA 98115.

Michael, K., L. A. Suberg, W. Wessels, S. Kawaguchi, and B. Meyer. 2021. Facing Southern Ocean warming: Temperature effects on whole animal performance of Antarctic krill (*Euphausia superba*). Zoology 146:125910.

Miller, D. M. 1984. Reducing Transformation Bias in Curve Fitting. The American Statistician 38:124–126.

Morris, D. J., J. L. Watkins, C. Ricketts, F. Buchholz, and J. Priddle. 1988. An assessment of the merits of length and weight measurements of Antarctic krill *Euphausia superba*. British Antarctic Survey Bulletin 79:27–50.

Mueter, F. J., and M. A. Litzow. 2008. Sea ice retreat alters the biogeography of the Bering Sea continental shelf. Ecological Applications 18:309–320.

Nishizawa, B., K. Matsuno, E. A. Labunski, K. J. Kuletz, A. Yamaguchi, and Y. Watanuki. 2017. Seasonal distribution of short-tailed shearwaters and their prey in the Bering and Chukchi seas. Biogeosciences 14:203–214.

Pebesma, E. J. 2004. Multivariable geostatistics in S: the gstat package. Computers & Geosciences 30:683–691.

Phillips, E. M., D. Chu, S. Gauthier, S. L. Parker-Stetter, A. O. Shelton, R. E. Thomas, and O. R. Godo. 2022. Spatiotemporal variability of euphausiids in the California Current Ecosystem: insights from a recently developed time series. ICES Journal of Marine Science 79:1312–1326.

Pinchuk, A. I., and K. O. Coyle. 2008. Distribution, egg production and growth of euphausiids in the vicinity of the Pribilof Islands, southeastern Bering Sea, August 2004. Deep Sea Research Part II: Topical Studies in Oceanography 55:1792–1800.

RCoreTeam. 2025. R: A language and computing environment for statistical computing. R Foundation for Statistical Computing, Vienna, Austria. URL（https://www.R-project.org/〉.

Reiss, C. S., A. M. Cossio, V. Loeb, and D. A. Demer. 2008. Variations in the biomass of Antarctic krill (*Euphausia superba*) around the South Shetland Islands, 1996–2006. ICES Journal of Marine Science 65:497–508.

Ressler, P. H., A. De Robertis, and S. Kotwicki. 2014. The spatial distribution of euphausiids and walleye pollock in the Eastern Bering Sea does not imply top-down control by predation. Marine Ecology Progress Series 503:111–122.

Ressler, P. H., A. De Robertis, J. D. Warren, J. N. Smith, and S. Kotwicki. 2012. Developing an acoustic survey of euphausiids to understand trophic interactions in the Bering Sea ecosystem. Deep-Sea Research Part II 65–70:184–195.

Reynisson, P., A. Gislason, and G. L. Lawson. 2023. Concurrent observations of the euphausiid *Thysanoessa raschii* in an Icelandic fjord by acoustics and Video Plankton Recorder:

comparisons with theoretical models of target strength. Journal of Plankton Research 45:37–51.

Rooper, C. N., I. Ortiz, A. J. Hermann, N. Laman, W. Cheng, K. Kearney, K. Aydin, and V. Bartolino. 2021. Predicted shifts of groundfish distribution in the Eastern Bering Sea under climate change, with implications for fish populations and fisheries management. ICES Journal of Marine Science 78:220–234.

Sameoto, D. D. 1980. Quantitative measurements of euphausiids using a 120-kHz sounder and their in situ orientation. Canadian Journal of Fisheries and Aquatic Sciences 37:693–702.

Siddon, E. 2024. Ecosystem Status Report 2024: Eastern Bering Sea, Stock Assessment and Fishery Evaluation Report. North Pacific Fishery Management Council, 1007 West 3rd Ave., Suite 400, Anchorage, Alaska 99501.

Simmonds, E. J., and D. MacLennan. 2005. Fisheries Acoustics: Theory and Practice, 2nd ed. Blackwell, Oxford, England.

Simonsen, K. A., P. H. Ressler, C. N. Rooper, and S. G. Zador. 2016. Spatio-temporal distribution of euphausiids: an important component to understanding ecosystem processes in the Gulf of Alaska and Eastern Bering Sea. ICES Journal of Marine Science 73:2020–2036.

Smith, J. N. 2010. Physical Characteristics of Bering Sea zooplankton and their use to parameterize an acoustic scattering model for euphausiids. M.S. Thesis, School of Marine and Atmospheric Sciences Stony Brook University, Stony Brook NY:96 pp.

Smith, J. N., P. H. Ressler, and J. D. Warren. 2013. A distorted wave Born approximation target strength model for Bering Sea euphausiids. ICES Journal of Marine Science 70:204–214.

Stanton, T. K. 1988. Sound scattering by cylinders of finite length. I. Fluid cylinders. The Journal of the Acoustical Society of America 83(1): 55-63.

Stanton, T. K., and D. Chu. 2000. Review and recommendations for the modelling of acoustic scattering by fluid-like elongated zooplankton: euphausiids and copepods. ICES Journal of Marine Science 57:793–807.

Stanton, T. K., D. Chu, P. H. Wiebe, and Clay, C.S. 1993. Average echoes from randomly oriented random-length finite cylinders: zooplankton models. Journal of the Acoustical Society of America 94:3463–3472.

Stienessen, S. C., A. McCarthy, T. Honkalehto, N. Lauffenburger, and S. Urmy. 2025. Results of the acoustic-trawl survey of walleye pollock (*Gadus chalcogrammus*) on the U.S. Bering Sea Shelf in June - August 2022 (DY2207). 2025. AFSC Processed Rep. 2025-01, 68 p. Alaska Fish. Sci. Cent., NOAA, Natl. Mar. Fish. Serv., 7600 Sand Point Way NE, Seattle WA 98115.

Svantemann, M.M., Kraft, B.A., Thompson, F.F., Zhang, G., and L.A. Krag. 2025. Automated krill body length estimation based on stereo camera images. ICES Journal of Marine Science 82(5).

Woillez, M., J. C. Poulard, J. Rivoirard, P. Petitgas, and N. Bez. 2007. Indices for capturing spatial patterns and their evolution in time, with application to European hake

(*Merluccius merluccius*) in the Bay of Biscay. ICES Journal of Marine Science 64:537–550.